Thermal and exhumation history of the central Yorke Peninsula, southern Gawler Craton

Thesis submitted in accordance with the requirements of the University of Adelaide for an Honours Degree in Geology/Geophysics/Environmental Geoscience

Christine Thompson

November 2013

THE UNIVERSITY of ADELAIDE

THERMAL AND EXHUMATION HISTORY OF CENTRAL YORKE PENINSULA

ABSTRACT

The central Yorke Peninsula, South Australia, is a prospective area for iron-oxide-copper-gold mineralisation. However due to minimal exposure there is limited data on the metamorphic, deformation and cooling history on the Central Yorke Peninsula in southern Gawler Craton in southern Australia.

Here we use metamorphic zircon and monazite grains from drill holes in the Equis and Ranald prospects to determine the thermal history of the area. U-Pb geochronology suggests that central Yorke Peninsula underwent metamorphism during ca 1540 – 1480 Ma. Pressure – temperature (P-T) modelling suggests that the metamorphic conditions for this thermal event were high temperature/low pressure, amphibolite-granulite facies associated with normal to elevated geothermal gradients. The tectonothermal driver for this event is not clear, it can be suggested that a combination of extension and magmatism may be have contributed to this thermal event. After the thermal event the central Yorke Peninsula underwent a period of extension and exhumation.

Exhumation and extension was most likely accommodated by the Pine Point Fault during ca 1500 – 1450 Ma and was likely to be associated with reactivation of major structures, brittle faulting and regional folding in the Gawler Craton.

Ca 1600 – 1570 Ma Hiltaba-age mineralisation has possibly been affected by the ca 1540 to 1480 thermal event in ways of remobilisation and concentration and following that was possibly redistributed along the Pine Point Fault during the ca 1500 – 1450 Ma extension and exhumation.

KEYWORDS

Tectonothermal history
MnNCKFMASHTO
Yorke Peninsula
Gawler Craton
Monazite
Metamorphic
Proterozoic

TABLE OF CONTENTS

LIST OF FIGURES AND TABLES

INTRODUCTION

During the Proterozoic, basement rocks of the Gawler Craton (Fig. 1) were affected by a sequence of events: The Kimban Orogeny (ca 1730-1690 Ma: Hoek and Schaefer, 1998; Hand *et al.*, 2007); the Early Kararan Orogeny (ca 1690-1670 Ma: Daly *et al.*, 1998); the Hiltaba event (ca 1600 -1570 Ma: Betts *et al.*, 2002; Betts and Giles, 2006); the Late Kararan Orogeny (ca 1565-1540 Ma: Daly *et al.*, 1998; Betts and Giles, 2006); the Wartaken event (1500 Ma – 1450 Ma: Parker and Lemon, 1982) and the Coorabie Orogeny (1470 -1450 Ma: Direen *et al.*, 2005; Hand *et al.*, 2007). The Hiltaba Event in the Gawler Craton was a thermal event characterized by high-temperature/low pressure metamorphism and deformation associated with the intrusion of the ca. 1600 - 1580 Ma (Betts *et al.*, 2002) Hiltaba Granite Suite and extrusion of the ca. 1592 Ma (Fanning *et al.*, 1988) Gawler Range Volcanics (Daly *et al.*, 1998). Although variably deformed, the Hiltaba Granite Suite locally bears a metamorphic foliation, is altered and intrudes metasomatically altered assemblages.

Metasomatic assemblages associated with intrusion of the Hiltaba Granite Suite have been demonstrably linked to iron-oxide-copper-gold (IOCG) mineralisation throughout the Gawler Craton (e.g. Olympic Dam: e.g. Pollard, 2006). Conor *et al.* (2010) suggests that the emplacement of Hiltaba Suite intrusions (Arthurton and Tickera Granites) is a likely driver for alteration and IOCG mineralisation in the Moonta -Wallaroo district in southern Gawler Craton (central Yorke Peninsula: Fig 1). IOCG mineralisation in the Moonta-Wallaroo district is hosted by the ca 1765 - 1735 Ma (Conor, 1995; Skirrow *et al.*, 2007) Wallaroo Group, which is a package of variably deformed and metamorphosed siltstone-dominated metasedimentary and volcanic rocks (Conor, 1995; Cowley *et al.*, 2003).

Following intrusion of the Hiltaba Granite Suite in the Gawler Craton two tectonothermal events have been recognised during the ca 1500 – 1450 Ma period. These are the ca 1500 – 1450 Ma Wartaken event in the south-eastern Gawler Craton (Parker and Lemon, 1982; Webb *et al.*, 1986) and the ca 1470 – 1450 Ma Coorabie event in the north-western Gawler Craton (Direen *et al.*, 2005; Hand *et al.*, 2007). These events are characterised by brittle faulting and regional folding (Wartaken event: Parker and Lemon, 1982; Fanning *et al.*, 1988) and the reactivation of shear zones at greenschist to amphibolite facies, regional cooling and lithospheric (Coorabie Orogeny: Direen *et al.*, 2005; Hand *et al.*, 2007; Betts *et al.*, 2002; Betts and Giles, 2006). The tectonic drivers of the Coorabie and Wartaken orogenies are unclear (Direen *et al.*, 2005; Swain *et al.*, 2005; Hand *et al.*, 2007), however, Hand *et al.* (2007) suggests that reactivation of shear zones at this time were associated with regional denudation of the Gawler Craton.

Studies pertaining to the deformational and metamorphic history of the Yorke Peninsula are limited (Conor *et al.*, 2010), and the timing of the deformation events relative to peak metamorphism and the absolute conditions of peak metamorphism are unknown. Regional metamorphism ranges from upper greenschist facies in the north (e.g. Bute: Conor, 2002) to mid-amphibolite facies in the Wallaroo region (Fig. 2) (Conor *et al.*, 2010). Conor *et al.* (2010) reports that the Wallaroo Group has undergone two phases of deformation involving development of early isoclinal folds that were refolded by open upright folds (Conor *et al.*, 2010). The axial planes of the upright fold generation show evidence of amphibole-rich calc-silicate alteration that has been dated to give a minimum age of 1575 ± 6 Ma (Skirrow *et al.*, 2007; Conor *et al.*, 2010). This alteration is demonstrably associated with intrusion of the Hiltaba Granite Suite (Conor *et al.*, 2010). U-Pb dating of titanite samples from hydrothermal alteration within the Hillside

IOCG deposit (Fig. 2) gives an age of 1570 ± 8 Ma (Conor *et al.*, 2010) suggesting mineralisation is concurrent with intrusion of the Hiltaba Granite Suite, calc-silicate metasomatism and upright folding (Conor *et al.,* 2010). No evidence of hydrothermal alteration has been identified to be associated with the early isoclinal fold generation therefore this early fold event may not be associated with granite emplacement, mineralisation and metasomatism (Conor *et al.*, 2010). Based on this evidence Conor *et al.* (2010) suggests that the isoclinal fold generation was produced during the ca 1730 - 1690 Ma (e.g. Hoek and Schaefer, 1998) Kimban Orogeny. The later upright folds are more certainly related to the 1600 - 1570 Ma Hiltaba Event (Conor *et al.*, 2010).

IOCG mineralisation at the Hillside deposit has been shown to be controlled by the Pine Point Fault (Figure 2)(Conor *et al.*, 2010) which is a major structural feature that trends roughly north-south along the east coast of the Yorke Peninsula (Fig. 2). The influence of the Pine Point Fault on cooling and exhumation of rock packages on the Yorke Peninsula is unknown, as is whether the terrain cooled passively (i.e. slowly, after the termination of igneous intrusion with no uplift due to tectonism) or actively (i.e. increased cooling rates due to uplift via tectonism) (e.g. Stüwe and Ehlers, 1998). How exhumation and uplift may have been accommodated along the Pine Point Fault and how this potentially effected distribution of mineralisation at Hillside and elsewhere in the Yorke Peninsula is unknown.

With increased recent exploration activity for IOCG deposits in the Olympic Domain and in particular on the central Yorke Peninsula, an understanding of the details of geological events that have shaped the crust and their association with mineralisation is required. This study aims to elucidate the absolute timing and conditions of peak metamorphism and constrain the exhumation history of rock packages around the Hillside deposit and the Pine Point Fault on the central Yorke Peninsula. Bulk rock geochemistry of selected samples and metamorphic petrology will be utilized in the calculation of pressure-temperature paths to determine absolute metamorphic conditions. This will be combined with U-Pb monazite and zircon geochronology to constrain the timing of peak metamorphism. Additionally, the exhumation history and cooling rates of the region will be investigated using Ar/Ar biotite geochronology. The influence of activity along the Pine Point Fault and its effect on processes of ore genesis and distribution of potential additional mineral deposits on the Yorke Peninsula is discussed.

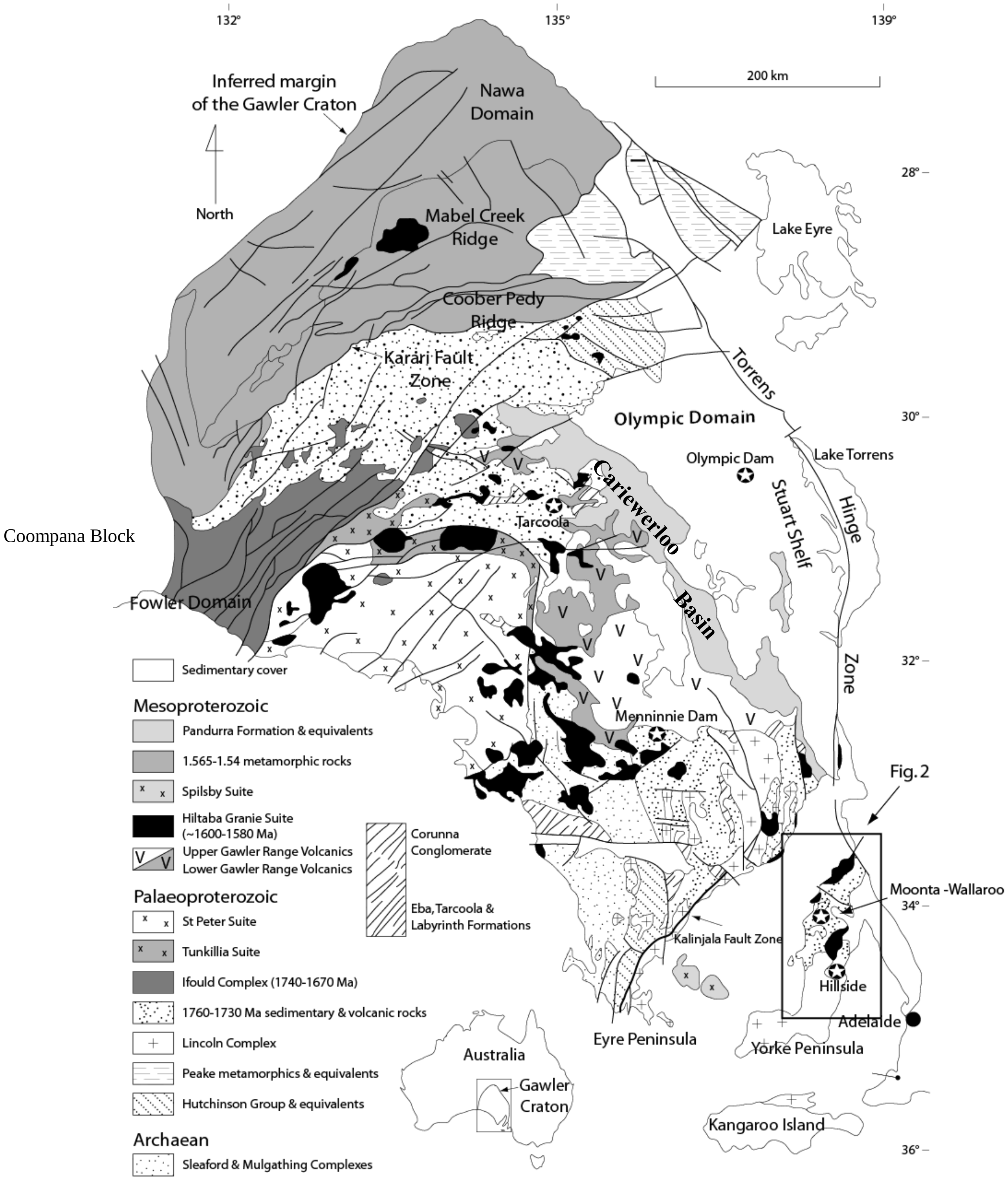

Figure 1

Figure 1 Geological map of the Gawler Craton showing IOCG deposits relating to the Hiltaba Event. The Yorke Peninsula is outlined and presented in Figure 2. Mineral Deposits are represented with stars. Modified after Daly *et al.* (1998).

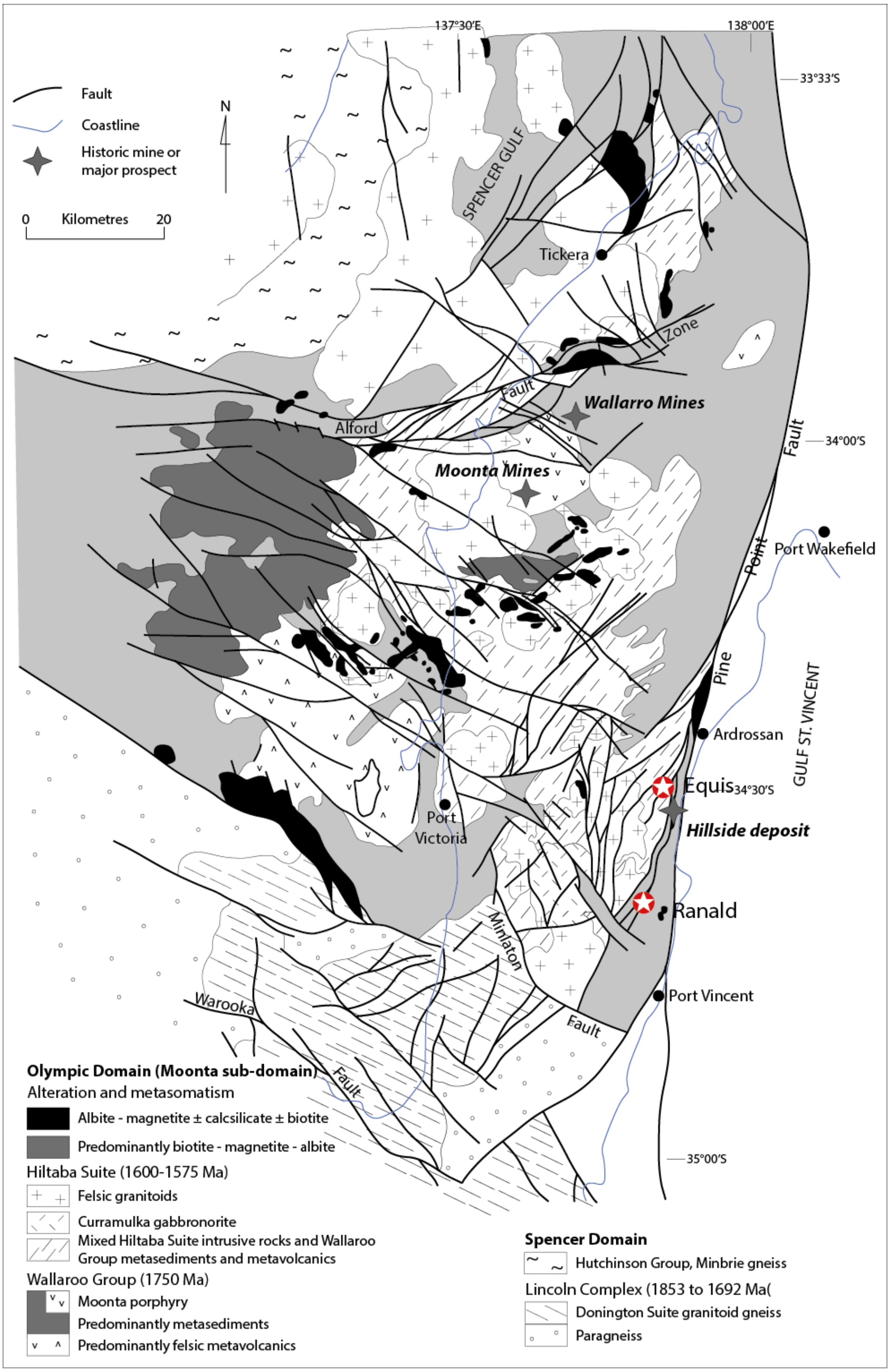

Figure 2Geological map of central Yorke Peninsula showing significant IOCG deposits and the location of the Pine Point Fault structural corridor. Locations of drill holes EQDD008A (Equis) and RDD003 (Ranald) are shown as red stars. Modified after Conor *et al.* (2010)

SAMPLE SELECTION

Samples locations (Fig. 2) for this study were selected for their proximity to the Hillside deposit and so that they were spatially separated enough so that any changes in metamorphic grade across central Yorke Peninsula would be apparent.

Samples were taken from diamond drill holes EQDD008A (approximately 10kms north of Hillside deposit; Fig. 2) and RDD003 (approximately 20kms south of Hillside deposit, Fig. 2) on the central Yorke Peninsula. Table 1 shows list of samples, location, lithology and work undertaken for this study. The samples were selected based on suitability for petrological and metamorphic analysis and for U-Pb zircon, monazite and biotite Ar/Ar geochronology. Samples were taken from EQDD008A at depths 397.3m (EQDD008A-397.3), 438.4m (EQDD008A-438.4) and 459.8m (EQDD008A-459.8). Five samples were taken from RDD003 at depths 262m (RDD003-262), 267.3m (RDD003-267.3), 292.2m (RDD003-292.2), 309.2m (RDD003-309.2) and 555.2m (RDD003-555.2). Samples from individual drill holes are thought to represent a single rock package as there are no evidence of structures between the individual Equis samples and the individual Ranald samples.

Sample	location	Depth(m)	Work undertaken	Lithology
EQDD008A-397.3	Equis	397.3	Biotite Ar/Ar geochronology, monazite geochronology	Sil-bt-ms-qtz-tur-kfs-pl-hem-mg gneiss
EQDD008A-438.4	Equis	438.4	monazite geochronology	Sil-bt-ms-qtz-tur-kfs-pl-hem-mg gneiss
EQDD008A-459.8	Equis	459.8	Biotite Ar/Ar geochronology, monazite geochronology, thin section petrography, P-T path	Sil-bt-ms-qtz-tur-kfs-pl-hem-mg gneiss
RDD003-262	Ranald	262	monazite geochronology	Crd-sil-bt-qtz-kfs-pl-hem-mg gneiss
RDD003-267.3	Ranald	267.3	monazite geochronology	Crd-sil-bt-qtz-kfs-pl-hem-mg gneiss
RDD003-292.2	Ranald	292.2	Biotite Ar/Ar geochronology, monazite geochronology	Crd-sil-bt-qtz-kfs-pl-hem-mg gneiss
RDD003-309.2	Ranald	309.2	Biotite Ar/Ar geochronology, monazite geochronology	Crd-sil-bt-qtz-kfs-pl-hem-mg gneiss
RDD003-555.2	Ranald	555.2	thin section petrography, P-T path	Crd-sil-bt-qtz-kfs-pl-hem-mg gneiss

Table 1 List of samples, location, lithology and analytical methods used. Localities shown in Fig. 2. Mineral abbreviations after Kretz (1983)

PETROLOGY

Detailed petrology was conducted on samples EQDD008A-459.8 and RDD003-555.2 as these were selected for pressure-temperature analysis. Hand specimens of these samples shown in Fig. 3.

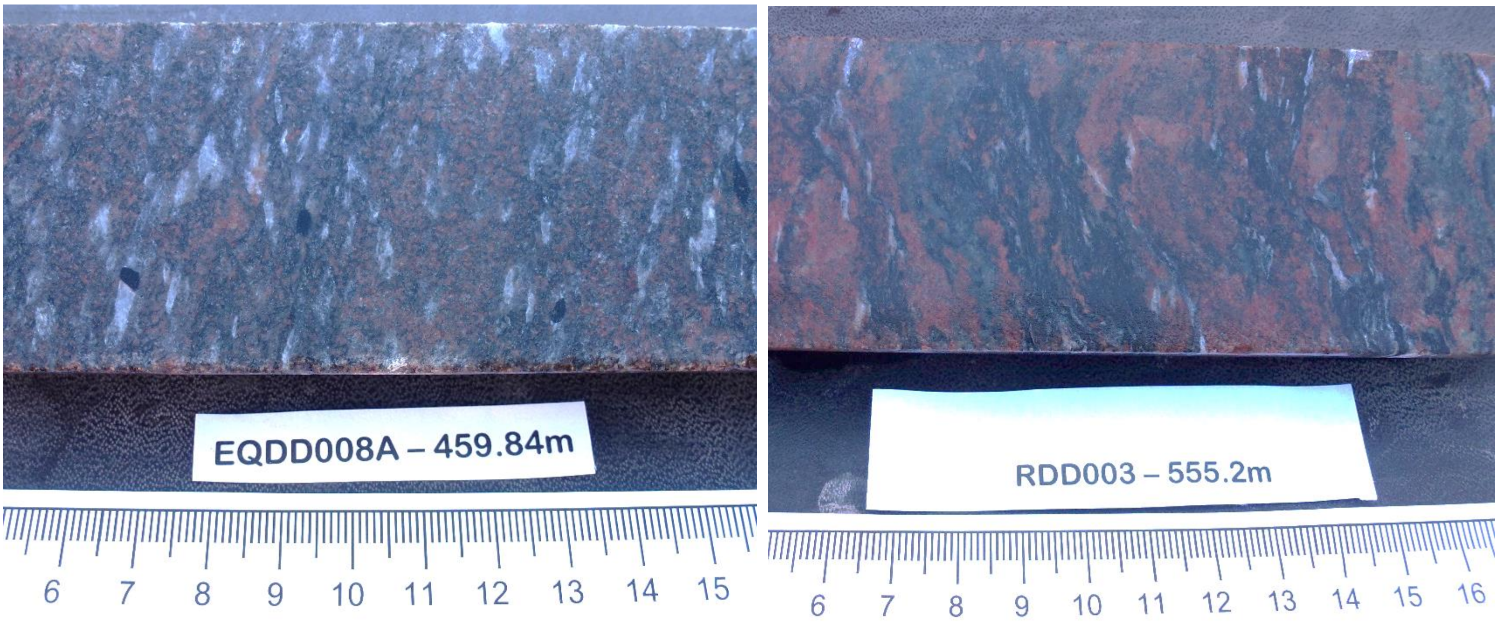

Figure 3 Hand specimens of samples (a) EQDD008A-459.8; (b) RDD003-555.2. Localities shown in Fig 2.

EQDD008A-459.8

The earliest assemblage recognised in sample EQDD008A-459.8 is an inclusion assemblage comprising of rounded opaques (5 to 15µm), quartz (5 - 15µm) and minor platy biotite (5 - 15µm) (Fig. 4).

The peak mineral assemblage comprises fibrolitic sillimanite-microcline-quartz-plagioclase-tourmaline-biotite-magnetite-haematite. Rare grains of tourmaline (<1% of whole rock) are preserved as large (2 to 4mm) idioblastic prismatic grains (Fig. 4). Fibrolitic sillimanite occurs within pressure shadows on the short edges of the tourmaline grains (Fig. 4). Fibrolitic sillimanite also forms lenses 2 to 7mm long (Fig. 4) and comprises 15% of the whole rock. The long axis of the fibrolite lenses defines a metamorphic foliation. An overprinting fabric can be seen as crenulations within the fibrolite lenses (Fig. 4).

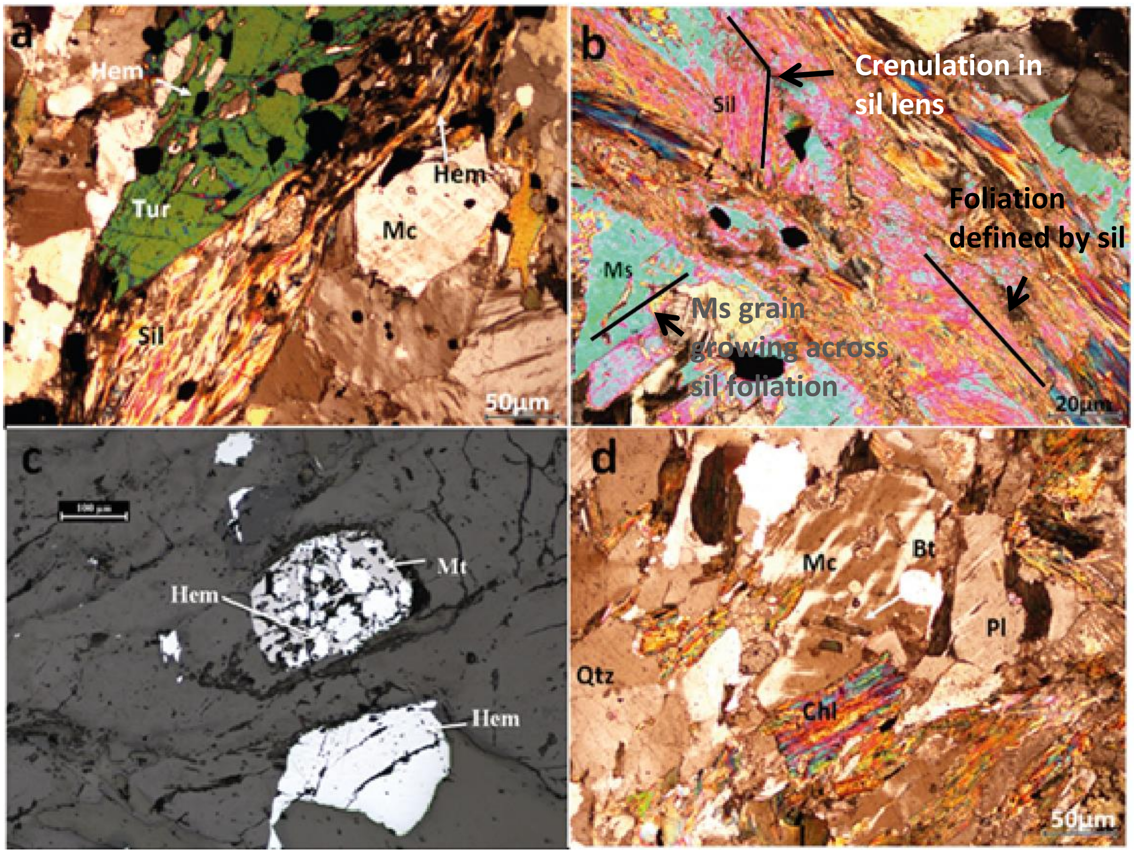

Figure 4 Photomicrographs of sample EQDD008A-E459.8. Abbreviations used are: Ms: muscovite; Sil: fibrolitic sillimanite; Bt: biotite; Hem: haematite; Mt: magnetite; Qtz: quartz; Mc: microcline; Pl: plagioclase feldspar; Tur: tourmaline; Chl: chlorite; (a) Rounded opaques and quartz inclusions can be seen in the tourmaline, microcline and quartz grains. Fibrolitic sillimanite forming a pressure shadow on the edge of the tourmaline grain; (b) Coarse grained muscovite is replacing a fibrolitic sillimanite lens and growing across the foliation defined by the lens; (c) Reflected light photomicrograph showing magnetite being partially replaced by haematite. The second haematite grain is completely haematite with no way to distinguish whether this represents a primary haematite grain or a completely replaced magnetite grain; (d) Photomicrograph of biotite being partially to completely replaced by chlorite. Sample locations shown in Fig. 2.

Xenoblastic quartz (30% of whole rock) grains are 20µm to 150µm and show undulose extinction. Microcline grains comprises ~17% of the whole rock, exhibits microcline twinning, are 50 to 150µm in size and have inclusions of rounded opaques, quartz and minor platy biotite (Fig. 4). Plagioclase grains (40-60µm) have albite twinning and comprise 10% of the whole rock. Idioblastic biotite grains are 40-250µm long and comprise 12% of the whole rock. Magnetite is rare (~0.5% of whole rock) with large

200 to 500µm grains. Magnetite shows moderate to major alteration to haematite along grain fractures (Fig. 4). Long tabular to acicular haematite grains, 10 to 100µm long, are present in (001) cleavage trace of biotite grains. Haematite makes up 4% of the total rock with the majority of the grains 50 to 300µm in size.

The sample is highly retrogressed with biotite being partially to completely replaced by chlorite. Sericite alteration is abundant throughout the sample and is prominent along fractures and twins in grains and on grain boundaries. Large (200µm to 1mm) platy muscovite grains replace fibrolite (Fig. 4) with muscovite grains cross cutting the metamorphic fabric (Fig. 4) and comprises 10% of the rock. Monazite grains are rounded, are 5 - 20µm in size and have rare simple twinning.

RDD003-555.2

The earliest mineral assemblage preserved in sample RDD003-555.2 is an inclusion assemblage of rounded haematite and quartz grains (Fig. 5). Idioblastic biotite is preserved as small 10µm idioblastic inclusions in quartz and cordierite (Fig. 5).

The peak mineral assemblage of this sample is fibrolitic sillimanite-microcline-plagioclase-quartz-biotite-magnetite-haematite. Microcline is 30 to 400µm in size and constitutes 20% of the whole rock. Microcline grains are poikoblastic, exhibits microcline twinning and contain inclusions of rounded opaques and quartz (Fig. 5). Xenoblastic 10µm - 100µm plagioclase comprises 4% of the whole rock. Grains preserve albite twinning and have inclusions of rounded opaques.

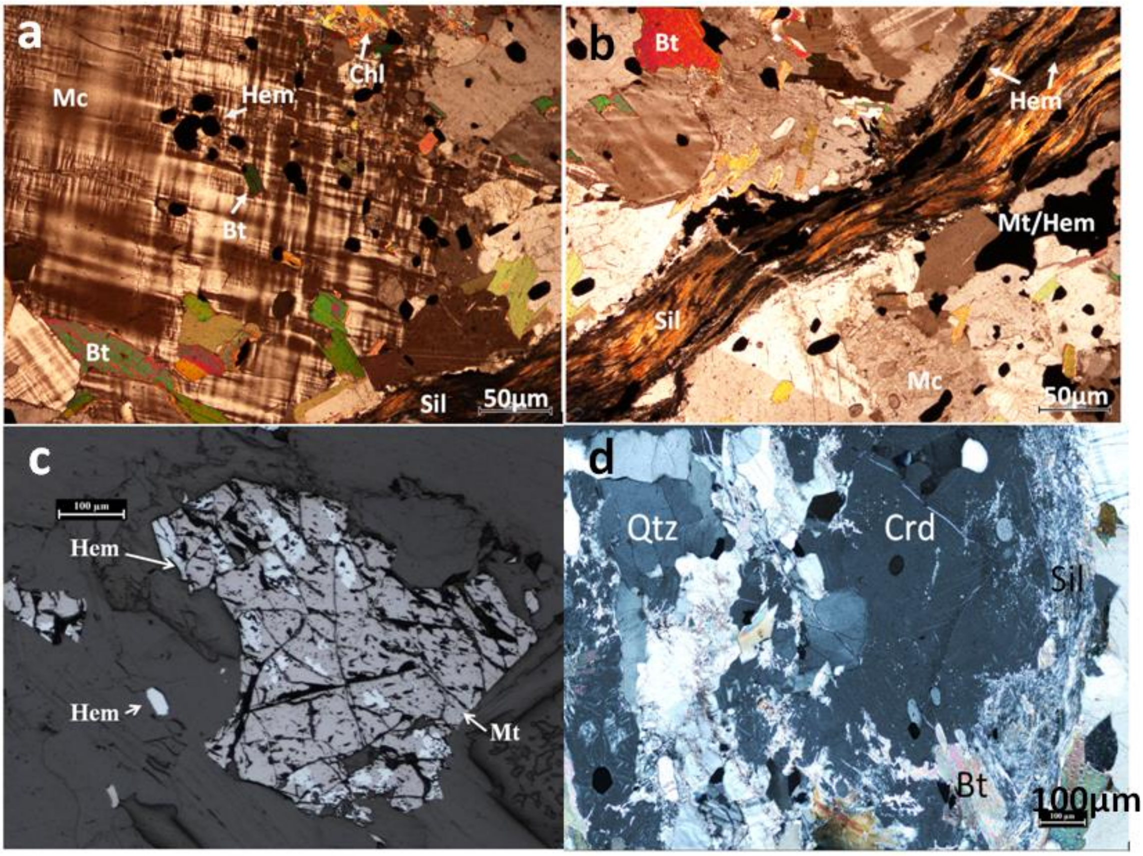

Figure 5 Photomicrographs of sample RDD003-555.2. Abbreviations used are: Ms: muscovite; Sil: fibrolitic sillimanite; Bt: biotite; Hem: haematite; Mt: magnetite; Qtz: quartz; Mc: microcline; Chl: chlorite; Crd: cordierite; (a) Rounded opaques, quartz and idioblastic biotite inclusions can be seen in the poikoblastic microcline grains. Fibrolitic sillimanite lens can be seen in the bottom right corner. Biotite altered to chlorite in top right corner; (b) Shows a fibrolitic sillimanite lens running through the centre of the photomicrograph. Elongate haematite grains are caught up in the fabric defined by the fibrolitic sillimanite lens; (c) Reflected light photomicrograph showing magnetite (dark grey) being partially replaced by haematite (bright grey). The second haematite grain is completely haematite with no way to distinguish whether this represents a primary haematite grain or a completely replaced magnetite grain; (d) Large cordierite grains are actively replacing fibrolitic sillimanite lens. Sample locations shown in Fig. 2.

Fibrolitic sillimanite (8% of the whole rock) forms lenses that are 5mm to 25mm long (Fig. 5) and define the earliest fabric recognised in the sample. A second fabric can be seen as crenulations within the fibrolitic sillimanite lenses (Fig. 5). Fibrolitic sillimanite grains are acicular 10µm -30µm in length and a dirty brown colour in plane polarised light. Biotite (10% whole rock) in this sample is pleochroic from straw yellow to a deep chocolate brown. The larger (up to 150µm) idioblastic grains tend to be parallel to the foliation defined by the fibrolite lenses (Fig 5).

Xenoblastic 100 – 750µm magnetite (0.5% of whole rock) grains are variably altered to haematite (Fig 10). These grains show abundant fracturing and have unstable boundaries. Haematite (2% whole rock) grains are either rounded 5 – 50µm and found throughout the sample or are xenoblastic and elongate and occur sub-parallel to the fabric defined by fibrolitic sillimanite lens (Fig. 5).

The peak mineral assemblage is overprinted by cordierite. Cordierite grains are large (30 to 500µm) and preserve a poikoblastic texture with inclusions of rounded quartz, opaques, and idioblastic fibrolitic sillimanite and biotite. Cordierite comprises 30% of the whole rock. Cordierite grains show retrogressive alteration to pinnite along fractures in the grains and along grain boundaries. Fig. 5 shows cordierite overprinting a fibrolitic sillimanite lens. Biotite is partially pseudomorphed by chlorite (Fig. 5). Sericite alteration is present in the sample with alteration along fractures in grains and the boundaries of grains. Monazite is the dominant accessory phase and occurs as rounded grains up to 10 – 20µm.

MINERAL CHEMISTRY

Microprobe analyses were obtained for samples RDD003-555.2 and EQDD008A-459.8 on the Cameca SX51 Electron Microprobe located at Adelaide Microscopy, University of Adelaide. Spot analyses were conducted using a beam current of 20nA and an accelerating voltage of 15 kV, with a defocused beam of 5 micron. Calibration was done on natural and synthetic mineral standards supplied by Astimex, Taylor, and P&H. Representative individual mineral compositions are given in for samples EQDD008A-459.8 and RDD003-555.2 in Tables 2 and 3 respectively.

EQDD008A-459.8

Feldspar

Plagioclase feldspars show minor compositional variation and is dominantly albite with X_{ab} (Na/Ca+ Na+ K) = 0. 44 – 0.88. Alkali feldspars are predominantly microcline and show minor compositional variation with X_{or} (K/K+ Na+ Ca) = values of 0.77 – 0.97.

Biotite

Biotite grains in this sample show minor compositional variation with X_{Fe} (Fe^{2+}/Fe^{2+} + Mg) = 0.32 – 0.8. Ti ranges from 0.004 to 0.72 cations per formula unit (p.f.u).

RDD003-555.2

Feldspar

Alkali feldspars show minor compositional variation and have X_{or}= values of 0.89 – 0.98 and combined with the crosshatched twinning under cross polarisation (figure 5) are predominantly microcline. Plagioclase feldspars show minor compositional variation and is dominantly albite with X_{ab} = 0.70 – 0.77.

Biotite

Biotite grains composition show minor variation with X_{Fe} (Fe^{2+} /Fe^{2+} + Mg) = 0.28 – 0.34. Ti in this sample ranges from 0.002 to 0.097 cations p.f.u.

Cordierite

Cordierite is highly pinnitised which explains the high K values. The samples analysed shows minor compositional variation with an average X_{Mg} (Mg/Mg+Fe^{2+}+Mn) = 0.69.

Spot Number	E459.8 - Bi_3	E459.8 - Kspar_3	E459.8 - Sill_4	E459.8 - Plag_4	E459.8 - Op_6	E459.8 - Mus_5
Expected mineral	Bi	Kspar	Sill	Plag	hem	Mus
SiO2	35.3	64.3427	36.8758	57.7872	0.0003	46.3604
TiO2	1.2984	0.0002	0.0179	0.0002	20.3193	0.3778
Al2O3	18.3511	18.7227	62.1545	26.1334	0.0003	34.8217
Cr2O3	0.0476	0.0671	0.167	0.0672	0.3463	0.0497
FeO	14.5535	0.0478	0.6073	0.0989	77.5294	3.1413
MnO	0.2907	0.0002	0.0034	0.0276	0.7905	0.0002
MgO	15.2475	0.0002	0.0142	0.0124	0.1306	0.8764
CaO	0.051	0.047	0.0247	8.2969	0.0279	0.0002
Na2O	0.2131	0.9975	0.0386	6.9717	0.1266	0.2372
K2O	8.7834	15.1961	0.0077	0.2337	0.0819	10.1395
ZnO	0.0002	0.0881	0.0052	0.0002	0.0989	0.0002
Total	94.1365	99.5096	99.9163	99.6294	99.452	96.0046
number of oxygen	11	8	5	8	3	11
Si	3.083951407	3.196568	1.188081	2.866026	1.28E-05	3.487104
Ti	0.062604419	5.48E-06	0.000318	5.47E-06	0.477284	0.015684
Al	1.39012854	0.806516	1.736349	1.12384	1.11E-05	2.271056
Cr	0.002412516	0.001934	0.003121	0.001934	0.00855	0.002169
Fe3+						
Fe2+	0.769458864	0.001437	0.011841	0.002968	1.996899	0.142992
Mn	0.01578323	6.17E-06	6.81E-05	0.000851	0.020909	9.35E-06
Mg	1.457049003	1.09E-05	0.0005	0.000673	0.00608	0.072105
Ca	0.003502749	0.001836	0.000626	0.323497	0.000934	1.18E-05
Na	0.026484547	0.070498	0.001769	0.491885	0.007665	0.025381
K	0.718271232	0.706659	0.000232	0.010849	0.003263	0.713883
Zn	9.46429E-06	0.002371	9.07E-05	5.37E-06	0.00228	8.15E-06
Total	7.529655971	4.78784	2.942997	4.822533	2.523887	6.730403

Table 2 Representative mineral compositions from microprobe analyses for sample EQDD008A-459.8.

Spot Number	R555.2 - Bi_4	R555.2 - kspar_7	R555.2 - Plag_5	R555.2 - Sill_5	R555.2 - Op_3	R555.2cd.cd_1
Expected mineral	bi	kspar	plag	sill	Hem	cd
SiO2	37.0363	64.2065	59.9544	44.0268	0.0199	41.131
TiO2	1.7235	0.0002	0.0002	0.0002	57.6232	0.0002
Al2O3	19.6385	18.8751	25.2589	54.3003	0.0003	33.8725
Cr2O3	0.0002	0.1673	0.1173	0.1501	0.8801	0.008
FeO	11.8491	0.0626	0.1885	0.5672	35.6164	7.2876
MnO	0.0839	0.0069	0.0069	0.0002	0.0001	0.0563
MgO	15.6269	0.003	0.1535	0.0257	0.0123	6.8164
CaO	0.014	0.036	5.6639	0.0129	0.0086	0.3747
Na2O	0.1534	1.004	8.149	0.0002	0.0155	0.1301
K2O	9.713	14.9113	0.2467	0.0132	0.0201	2.8615
ZnO	0.0002	0.1497	0.0002	0.1247	0.0235	0.0002
Total	95.839	99.4226	99.7395	99.2215	94.22	92.5385
Number of Oxygen	11	8	8	5	3	14
Si	3.121877802	3.191283155	2.93332336	1.382225122	0.000694034	5.290163205
Ti	0.080179484	5.48631E-06	5.40048E-06	3.46542E-06	1.109146679	1.41969E-05
Al	1.435346175	0.813458949	1.071552244	1.478168446	9.07213E-06	3.777522767
Cr	9.78022E-06	0.00482406	0.00332941	0.002733838	0.017806984	0.000596926
Fe3+						
Fe2+	0.604447808	0.00188298	0.0055813	0.010776631	0.751732114	0.567243418
Mn	0.004395095	0.000213134	0.0002098	3.9022E-06	2.16743E-06	0.004500142
Mg	1.440800446	0.000163099	0.008214667	0.000882546	0.000469219	0.958953536
Ca	0.000927732	0.001406679	0.217851488	0.000318389	0.000235794	0.037886943
Na	0.018394583	0.070989862	0.567178126	8.9324E-06	0.000769017	0.023804188
K	0.766363276	0.693736974	0.011297986	0.000387908	0.000656171	0.344497871
Zn	9.13153E-06	0.004030262	5.30022E-06	0.002120573	0.000443937	1.39333E-05
Total	7.472751313	4.78199464	4.818549081	2.877629753	1.881965189	11.00519713

Table 3 Representative mineral compositions from microprobe analyses for sample RDD003-555.2.

PRESSURE TEMPERATURE PATHS

Bulk whole rock geochemical analysis was done on all samples (Table 1) for major element chemistry and is shown in Table 4. Titration analysis to determine the Fe^{2+} and Fe^{3+} content of samples EQDD008A-459.8 and RDD003-555.2 was also done (Table 5). All geochemical analyses were done by Genalysis Laboratory Services, Adelaide.

Samples RDD003-555.2 and EQDD008A-459.8 (Fig. 3) were selected as the most suitable samples for calculating pressure–temperature (P-T) pseudosections as geochemistry results were closest out of all the samples to the standard metapelite geochemistry. P-T analysis will be used to visualise multivariant mineral assemblages and to constrain the thermal evolution of the central Yorke Peninsula. THERMOCALC v.3.33 was used to calculate the pseudosections in the model system MnO–NaO–CaO–K_2O–FeO–MgO–Al_2O_3–SiO_2–H_2O–TiO_2-O (MnNCKFMASHTO).
Due to the presence of magnetite ($Fe^{2+}Fe^{3+}{}_2O_4$) and haematite (Fe_2O_3) in the samples, both Fe^{2+} and Fe^{3+} were required to be modelled. Modelled content was taken from tritation analysis results (Table 5). H_2O is taken to be in excess below the solidus and was set above solidus so the rocks are fluid saturated. The calculated pseudosections for EQDD008A-459.8 and RDD003-555.2 are shown in Figures 6 and 7 respectively. Mineral abbreviations are after Kretz (1983).

ELEMENTS	EQDD008A-459.8*	RDD003-555.2*	RDD003-309.2	RDD003-267.3	RDD003-262	EQDD008A-397.3	EQDD008A-438.4
SiO2	54.6	55.43	58.51	56.8	60.63	56.69	57.29
TiO2	0.85	0.83	0.85	0.78	0.8	0.77	0.68
Al2O3	20.14	19.92	18.16	19.86	18.84	18.72	18.65
Fe2O3	9.95	9.32	9.24	9.35	7.51	9.05	8.84
MnO	0.08	0.03	0.05	0.06	0.05	0.04	0.08
MgO	3.4	2.84	2.7	2.24	1.56	3.33	3.68
CaO	1.69	0.9	2.35	1.19	1.06	1.13	1.37
Na2O	1.75	1.75	2.32	1.42	1.43	2.16	1.91
K2O	5.79	6.58	3.66	6.66	5.94	5.63	5.81
Total	**98.25**	**97.6**	**97.84**	**98.36**	**97.82**	**97.52**	**98.31**
SiO2	65.63	67.26	69.25	68.52	72.32	67.81	67.64
TiO2	0.77	0.76	0.76	0.71	0.72	0.69	0.60
Al2O3	14.27	14.24	12.66	14.12	13.24	13.20	12.98
Fe2O3	4.50	4.25	4.11	4.24	3.37	4.07	3.93
	0.00	0.00	0.00	0.00	0.00	0.00	0.00
MnO	0.08	0.03	0.05	0.06	0.05	0.04	0.08
MgO	6.09	5.14	4.76	4.03	2.77	5.94	6.48
CaO	2.18	1.17	2.98	1.54	1.35	1.45	1.73
Na2O	2.04	2.06	2.66	1.66	1.65	2.50	2.19
K2O	4.44	5.09	2.76	5.12	4.52	4.30	4.38

Table 4 Bulk Chemistry for all samples collected. * Donates samples selected for pressure temperature pseudosection calculation. Sample locations shown in Fig. 2.

Sample	ELEMENTS	SiO2	TiO2	Al2O3	Cr2O3	Fe	FeO	MnO	MgO	CaO	Na2O	K2O	P	LOI	Total
EQDD008A-459.8		54.89	0.82	20.04	0.017	6.98	3.25	0.08	3.25	1.62	1.73	5.87	0.088	1.63	100.25
RDD003-555.2		56.54	0.81	19.21	0.018	6.63	2.34	0.02	2.68	0.91	1.76	6.69	0.064	1.8	100.25

Table 5 Titration analysis results for samples EQDD008A-459.8 and RDD003-555.2. Sample locations shown in Figure 2.

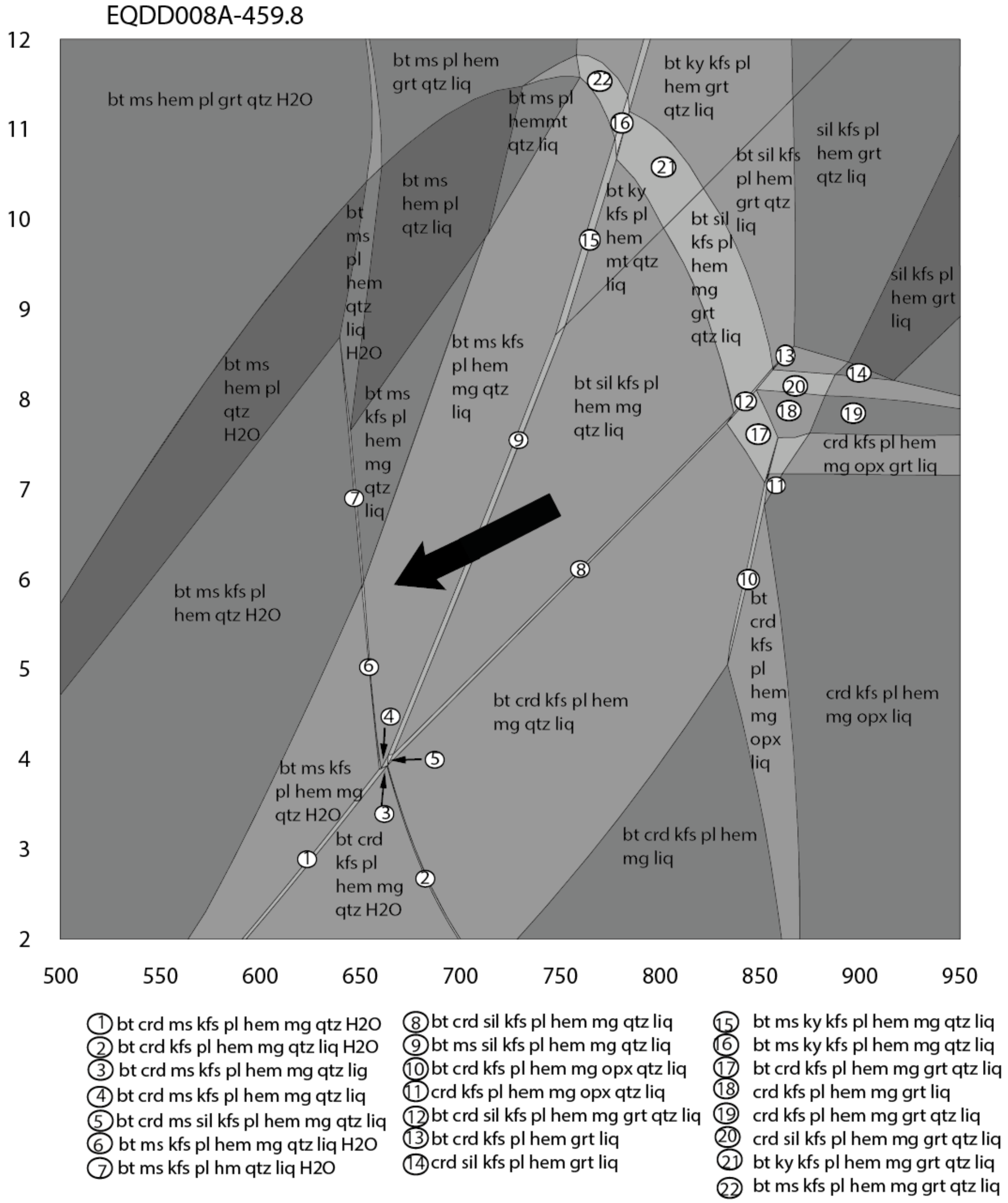

Figure 6 Pressure – Temperature (P-T) diagram for EQDD008A-459.8. Arrow represents interpreted P-T path. Mineral abbreviations are after Kretz (1983). Sample location shown in Figure 2.

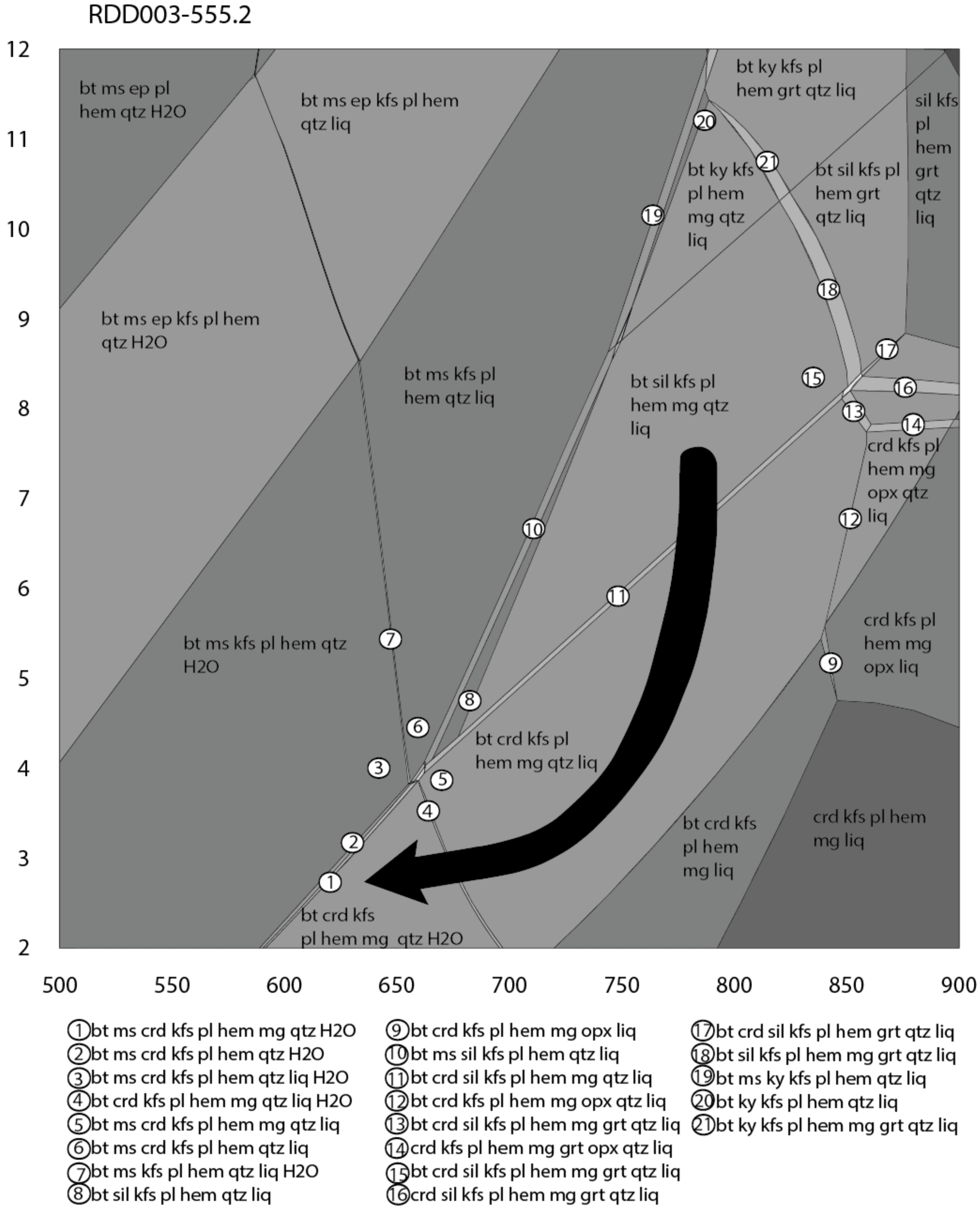

Figure 7 Pressure – Temperature (P-T) diagram of RDD003-555.2. Arrow represents interpreted P-T path. Abbreviations are after Kretz (1983). Sample location shown in Figure 2.

U-Pb GEOCHRONOLOGY

U-Pb monazite and zircon geochronology was undertaken via Laser Ablation Inductively Coupled Plasma Mass Spectrometry (LA-ICP-MS) at Adelaide Microscopy, University of Adelaide. Monazite grains from samples RDD003-267.3, RDD003-262, RDD003-292, RDD003-309.2, EQDD008A-397.3, EQDD008A-438.4, EQDD008A-459.8 and zircon grains from sample RDD003-292.2 were analysed to obtain constrained metamorphic ages of Central Yorke Peninsula. Sample localities are shown in Figure 2. The analytical technique for separation of monazite and zircon grains and the subsequent U-Pb dating is given in Appendix A.

Data for all zircon and monazite analysis are presented in Appendices C- J. Cathodeluminescence (CL) images of representative zircon grains analysed from sample RDD003-555.2 and backscattered electron (BSE) images of representative monazite grains from all samples are shown in Figures 8 and 9 respectively. Concordia, weighted average and probability density plots are shown with quoted errors at 95% confidence levels in Figures 10, 11 and 12 respectively.

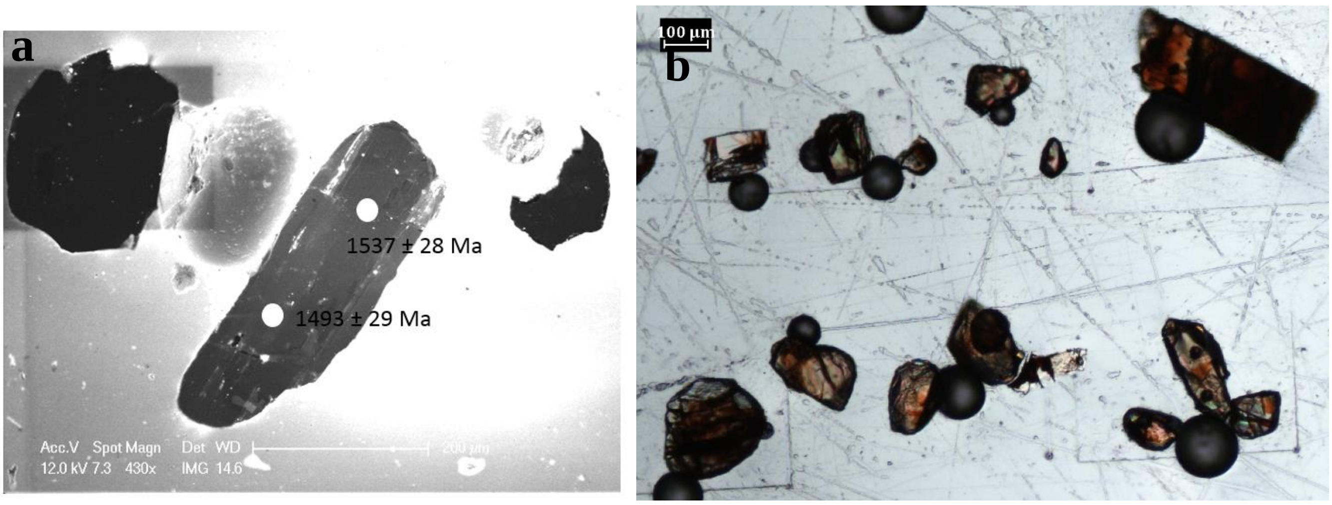

Figure 8 (a) Cathodeluminescence image of a representative zircon grain from sample RDD003-292.2; (b) Transmitted light image of zircon population. Sample location shown in Figure 2.

ton

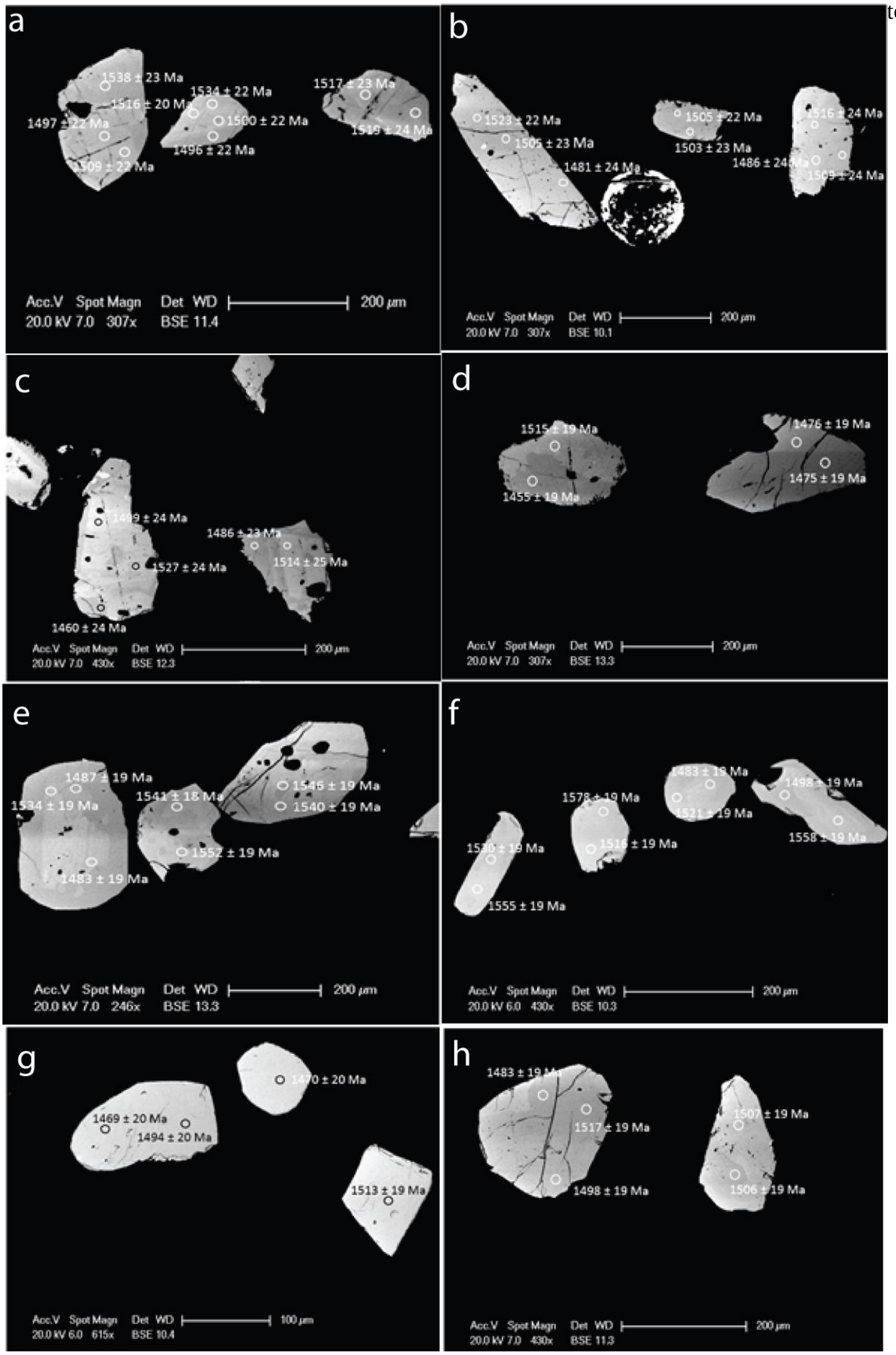

Figure 9 Back scattered electron (BSE) images of representative monazite grains from each sample analysed; (a) EQDD008A-397.3; (b) EQDD008A-438.4; (c) EQDD008A-459.8 Minor patchy zoning can be seen; (d) RDD003-267.3. Representative monazite grains from the 1477 ± 12 Ma age population. Minor patchy zoning can be seen in some grains; (e) RDD003-267.3. Representative monazites from the 1544 ± 9 Ma age population. Minor patchy zoning can be seen in some grains; (f) RDD003-262; (g) RDD0003-309.2; (h) RDD003-292.2. Minor patchy zoning can be seen in some grains. Sample localities are shown in Figure 2.

Zircon geochronology

RDD003-292.2

The zircon grains from sample RDD003-292.2 (Fig. 2) are bland and homogeneous in cathodeluminescence imaging (Fig. 8a) with rare patchy zoning which does not correspond to age differences. The zircon grains are yellow and cloudy with a red staining in transmitted light (Fig. 8b). Grains vary from 50µm to 400µm in length and round to sub round in shape.

Twenty-eight zircons with a total of 47 spot analyses were analysed from sample RDD003-292.2 (Figs 2 and 10). 5 data points were removed from age calculations due to radiogenic lead loss (Fig. 10a). The Th/U ratios for the zircon grains analysed range in value of 0.1 to 0.9 with an average Th/U ratio of 0.71 (Appendix C).

While at first glance there appears to be a bimodal distribution on ages with ages of 1558 ± 7 Ma (MSWD= 0.51) and 1498 ± 8 Ma (MSWD= 0.49) (Fig. 10b), there is no clear morphological evidence in the zircon grains to differentiate the analyses and so after removing the radiogenic lead loss analyses, the data distribution becomes unimodal with a weighted average of 1538 ± 13 Ma (MSWD= 1.6) (Fig. 10a).

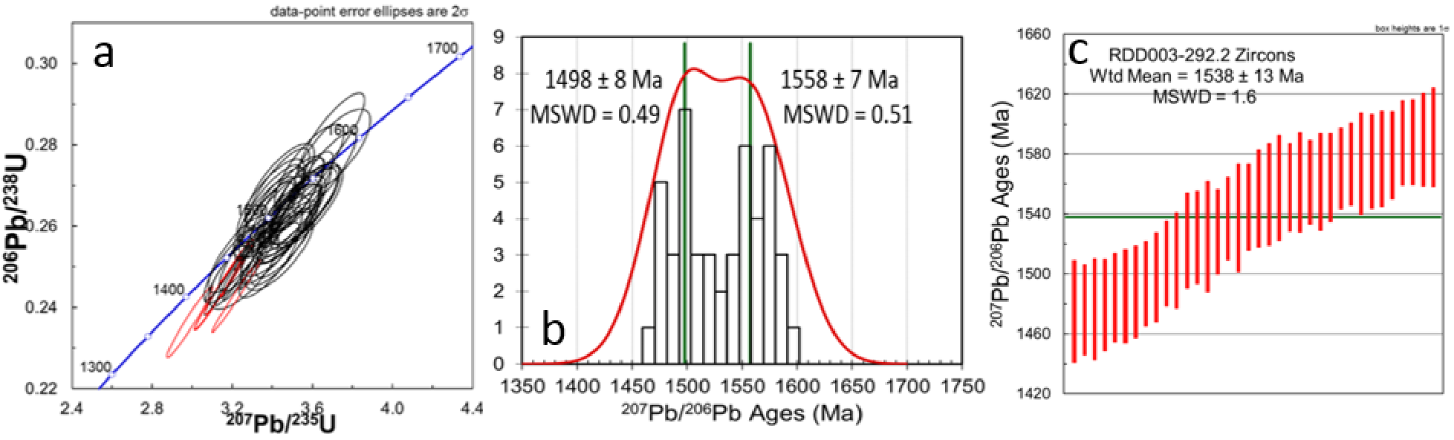

Figure 10 U-Pb results for RDD003-292.2 zircon grain analysis. Age shown as a weighted (Wtd) average; (a) Concordia diagram. Red circles indicate excluded from final analyses due to radiogenic lead loss; (b) probability density plot of total analyses showing two possible populations at 1498 ± 8 Ma and 1558 ± 7 Ma; (c)Weighted average plot of recorded analyses after analyses showing radiogenic lead loss were removed. Shows one population with a Wtd average of 1538 ± 13 Ma. Sample location shown in Figure 2.

Monazite Geochronology

Equis

EQDD008A-397.3

Monazite grains from sample EQDD008A-397.3 are round to sub round and clear in transmitted light. The grains are 50µm to 300µm in length. The backscattered electron (BSE) images (Fig. 9a) of the samples show broad homogeneous internal structure and a lack of igneous zonation. Mottling (dark and light patches) show minor uranium compositional zoning however these zones do not correspond to age distribution. Twenty monazites were analysed from sample EQDD008A-397.3 with a total of 46 analyses (Appendix D). The $^{207}Pb/^{206}Pb$ age data show a unimodal age distribution (Fig. 11a). Weighted average analyses of $^{207}Pb/^{206}Pb$ age data yield an age of 1518± 7 Ma (MSWD=0.96)

EQDD008A-438.4

Monazite grains from sample EQDD008A-438.4 are round to sub round and clear in transmitted light. The grains are 100µm to 400µm in length. The backscattered electron (BSE) images of the samples show broad homogeneous internal structure and a lack of igneous zonation and have numerous inclusions (Fig. 9b). Mottling (dark and light patches) show minor uranium compositional zoning however these zones do not correspond to age distribution. Thirty monazites were analysed from sample EQDD008A-438.4 with a total of 66 analyses (Appendix E). Four data points were removed due to radiogenic lead loss. The $^{207}Pb/^{206}Pb$ ages show a unimodal distribution (Fig.11c). Weighted average analyses of $^{207}Pb/^{206}Pb$ age data yield an age of 1500 ± 7 Ma (MSWD=1.3)

EQDD008A-459.8

Monazite grains from sample EQDD008A-459.8 are round to sub round and clear in transmitted light. The grains are 80μm to 300μm in length. The backscattered electron (BSE) images of the samples show broad homogeneous internal structure, a lack of igneous zonation and multiple inclusions (Fig. 9c). Mottling (dark and light patches) show minor uranium compositional zoning however these zones do not correspond to age distribution. Seventeen monazites were analysed from sample EQDD008A-459.8 with a total of 35 analyses (Appendix F). The $^{207}Pb/^{206}Pb$ ages show a unimodal distribution (Fig. 9d). Weighted average analyses of $^{207}Pb/^{206}Pb$ age data yield an age of 1495 ± 8 Ma (MSWD=1.07) (Fig. 11f).

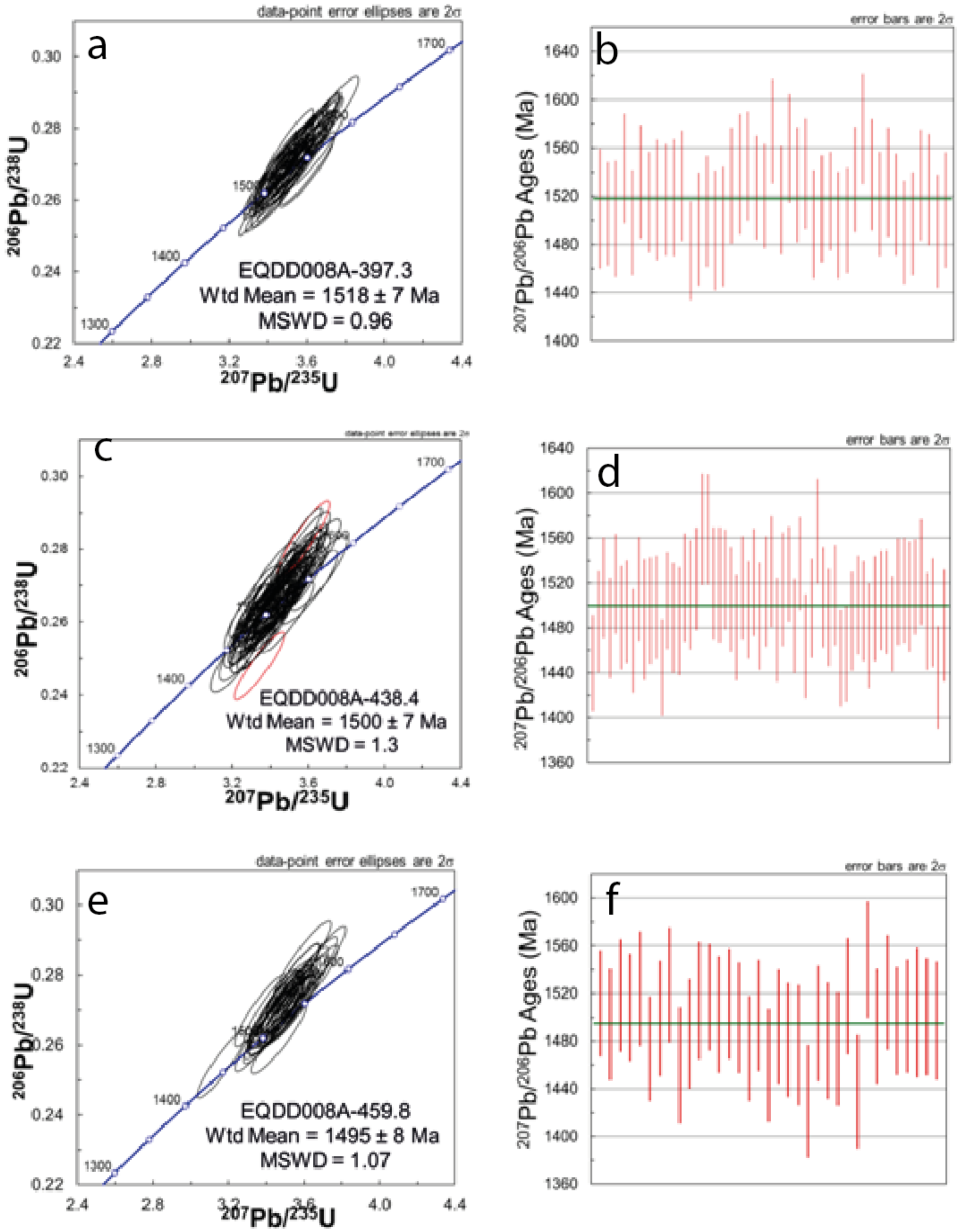

Figure 11 Results for Equis monazite samples presented as concordia plots and weighted average plots. Excluded data is represented as red circles in concordia plots. All ages quoted are ^{207}Pb/^{206}Pb Ages (Ma) and are weighted (Wtd) averages; (a) EQDD008A-397.3 concordia plot showing one age population at 1518 ± 7 Ma; (b) EQDD008A-397.3 weighted average plot; (c) EQDD008A-438.3 concordia plot showing one age population at 1500 ± 7 Ma. Excluded analysis highlighted in red; (d) EQDD008A-438.4 weighted average; (e) EQDD008A-459.8 concordia plot showing one age population at 1495 ± 8 Ma; (f) EQDD008A-459.8 weighted average.

Ranald

RDD003-262

Monazite grains from sample RDD003-262 are 80µm to 200µm in length. Twenty-two monazites were analysed from sample RDD003-262 with a total of 37 analyses (Appendix G). Five data points rejected due to radiogenic lead loss. Whilst patchy compositional zoning is present in some grains (Fig. 9f), there is no apparent correlation between age distribution and zoning. Weighted average analyses yield ages of 1533 ± 9 Ma (MSWD=1.5) (Fig. 12a).

RDD003-267.3

Monazite grains from sample RDD003-267.3 are 150µm to 500µm in length. Eighteen monazite grains were analysed from sample RDD003-267.3 with a total of 37 analyses (Appendix H). One data point was removed due to discordance. Compositional zoning is evident in the BSE images (Fig. 9d) with the older ages consistently associated with the light zoned patches. The $^{207}Pb/^{206}Pb$ age data indicate a bimodal distribution. Weighted average analyses yield ages of 1477 ± 12 Ma (MSWD=0.71) and 1544 ± 9 Ma (MSWD=1.5) (Fig. 12c).

RDD003-292.2

Monazite grains from sample RDD003-292.2 are 50µm to 200µm with one grain 300µm in length. Multiple fractures are evident in the grains (Fig. 9e). Twenty-two monazites were analysed from sample RDD003-292.2 with a total of 36 analyses (Appendix I). Three data points removed due to high ^{204}Pb values. A trimodal age data was obtained from this sample. By removing the lesser peaks (four data points) at 1570

Ma and 1600 Ma, the weighted average analyses of the majority of analyses yield ages of 1509 ± 8 Ma (MSWD=1.18) (Fig. 12e).

RDD003-309.2

Monazite grains from sample RDD003-309.2 are 40μm to 250μm. No compositional zoning is evident in the BSE images of the grains analysed (Fig. 9g). Thirty-two monazite grains were analysed from sample RDD003-309.2 with a total of 37 analyses (Appendix J). Two data points were removed due to high ^{204}Pb and discordance. The probability density plot of the ^{207}Pb/^{206}Pb age data (Fig. 12g) shows an asymmetric bell curve. Weighted average analyses yield ages of 1489 ± 8 Ma (MSWD=1.4) (Fig. 12h).

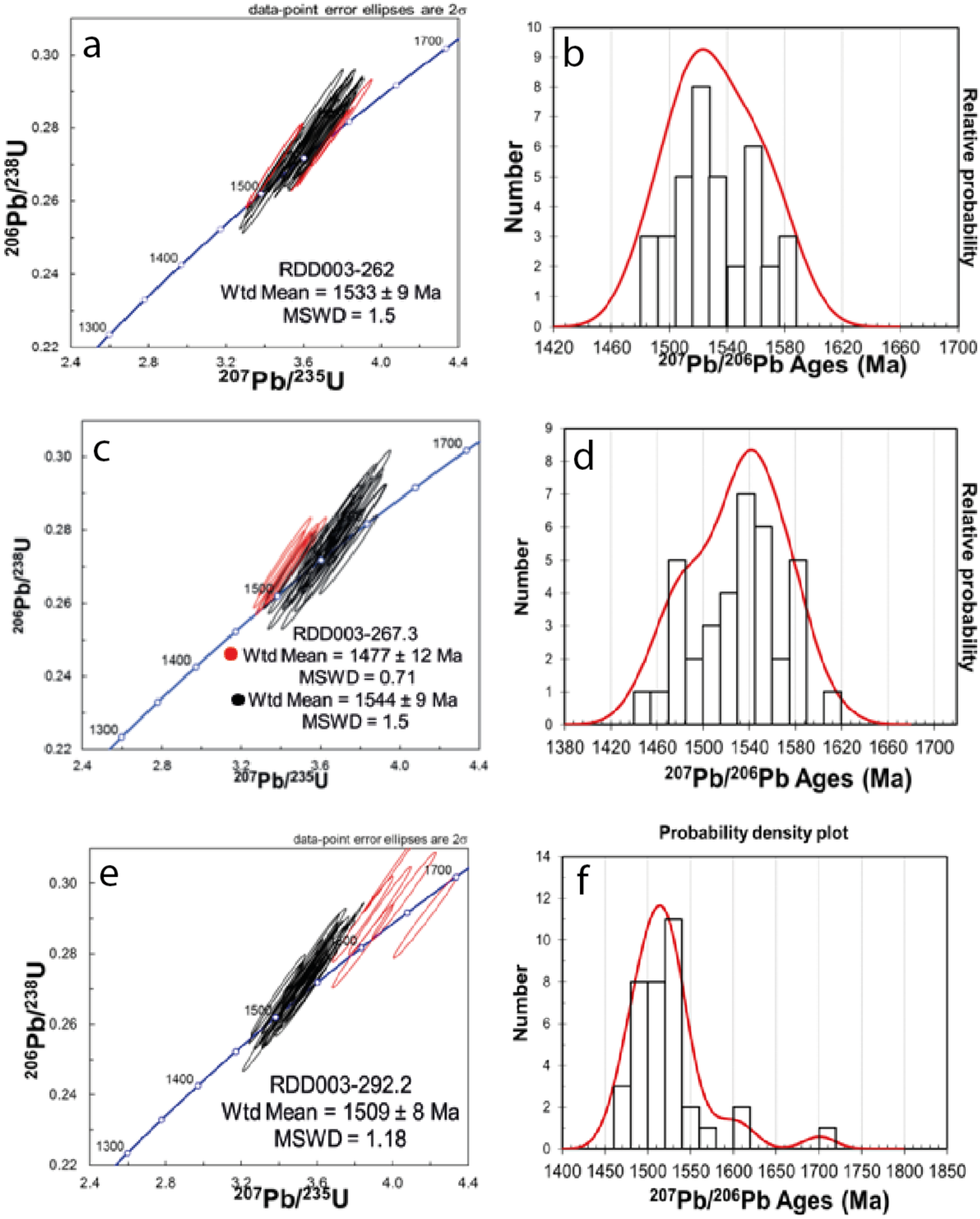

Figure 12 Results for Ranald monazite samples presented as concordia plots and probability density curves. All ages quoted are ^{207}Pb/^{206}Pb Ages (Ma) and are weighted (Wtd) averages; (a) RDD003-262 concordia plot with weight average age; (b) relative probability plot showing an asymmetric bell curve; (c) RDD003-267.3 concordia plot showing two age populations. Red concordia circles highlight the younger population at 1477 ± 12 Ma and the black circles highlighting the 1544 ± 9 Ma; (d) RDD003-267.3 relative probability curve showing two peaks which correspond to a younger and older age population; (e) RDD003-292.2 concordia plot. Excluded analysis highlighted in red; (f) RDD003-292.2 relative probability curve showing a trimodal age. The two smaller peaks were excluded from analysis for the main metamorphic event at 1509 ± 8 Ma; (g) RDD003-309.2 concordia plot. Red circles represent excluded data points. (h) probability density plot showing a bimodal age. Main age at 1489 ± 8 Ma. After removing the 2 lesser peaks, an asymmetric bell curve is recognised. Sample locality shown in Figure 2.

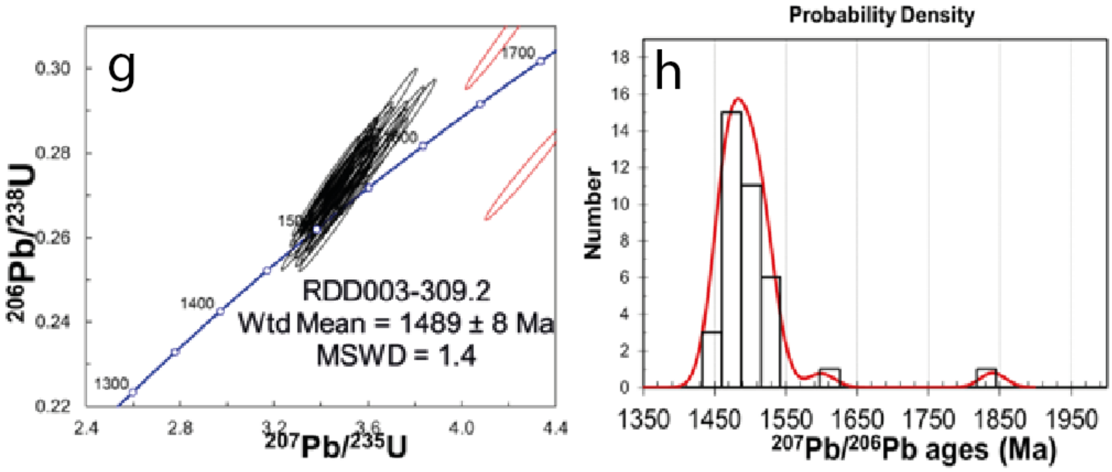

Figure 12 Continued.

BIOTITE Ar/Ar GEOCHRONOLOGY

Two samples each from drill holes EQDD008A (EQDD008A-397.3 and EQDD008A-459.8) and RDD003 (RDD003-292.2 and RDD003-309.2) were chosen for $^{40}Ar/^{39}Ar$ biotite dating to constrain the cooling age of central Yorke Peninsula. These samples were chosen as they preserve large fresh biotite grains (Fig. 13). All samples were also used for U-Pb monazite and zircon geochronology. Sample EQDD008A- 459.8 was used for P-T analysis (Fig. 6). Detailed sample preparation and analytical technique is outlined in Appendix B.

Biotite grains in sample EQDD008A-397.3 are idioblastic and 200μm to 2.5mm in size. The grains are aligned with the dominant foliation of the sample (Fig.13a).

Biotite grains from sample EQDD008A-459.8 are idioblastic, 400μm to 2.5mm long and are partially to completely altered to chlorite (Fig. 13b).

The biotite grains from sample RDD003-292.2 are platy and 500μm to 3mm in size (Fig. 13c). The grains are found in biotite-rich layers and are aligned with the dominant foliation of the sample.

The biotite grains from sample RDD003-309.2 are platy and 500µm to 3mm in size and are found in biotite rich layers in the sample (Fig. 13d). The grains are aligned with the dominant foliation of the sample and are part of the peak assemblage.

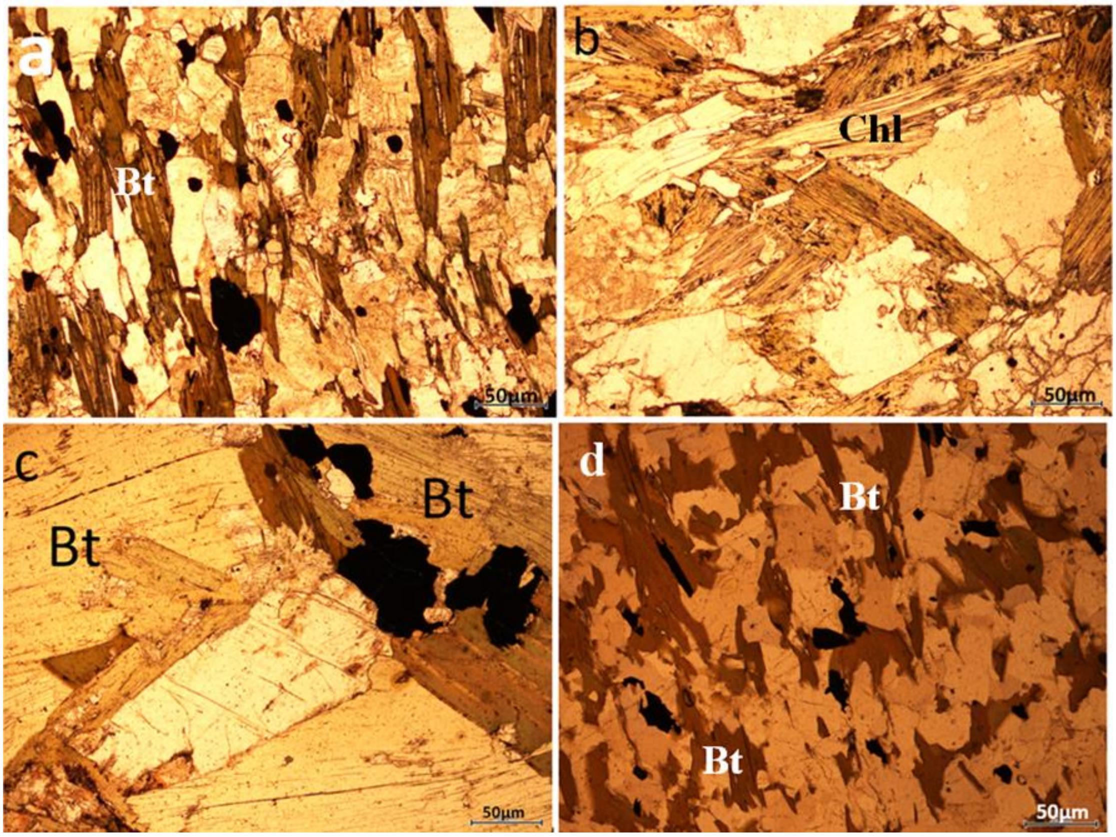

Figure 13 Photomicrographs of biotite from samples (a) EQDD008A-397.3; (b) EQDD008A-459.8; (c) RDD003-292.2 and (d) RDD003-309.2

Fig. 14 shows Ar/Ar data plotted against cumulative ^{39}Ar % for the four selected samples EQDD008A-397.3, EQDD008A-459.8, RDD003-292.2 and RDD003-309.2. 86% of ^{39}Ar released from EQDD008A-397.3, 95% of ^{39}Ar released from RDD003-292.2 and 75% of ^{39}Ar released from RDD003-309.2 was used in age calculation. No plateau was achieved from sample EQDD008A-459.8.

Samples EQDD008A-397.3, RDD003-292.2 and RDD003-309.2 yielded ages 1451±6Ma (P=0.92), 1455 ± 6 Ma (P=0.42) and 1466 ± 6 Ma (P=0.99). Ages for samples EQDD008A-397.3 and RDD003-292.2 are within error of each other and are considered indistinguishable. The low temperature steps give a maximum age for the latest heating events at ~ 1350-1300 Ma for samples EQDD008A-397.3 and RDD003-292.2 and younger than 1150 Ma for RDD003-309.3 (Fig. 14).

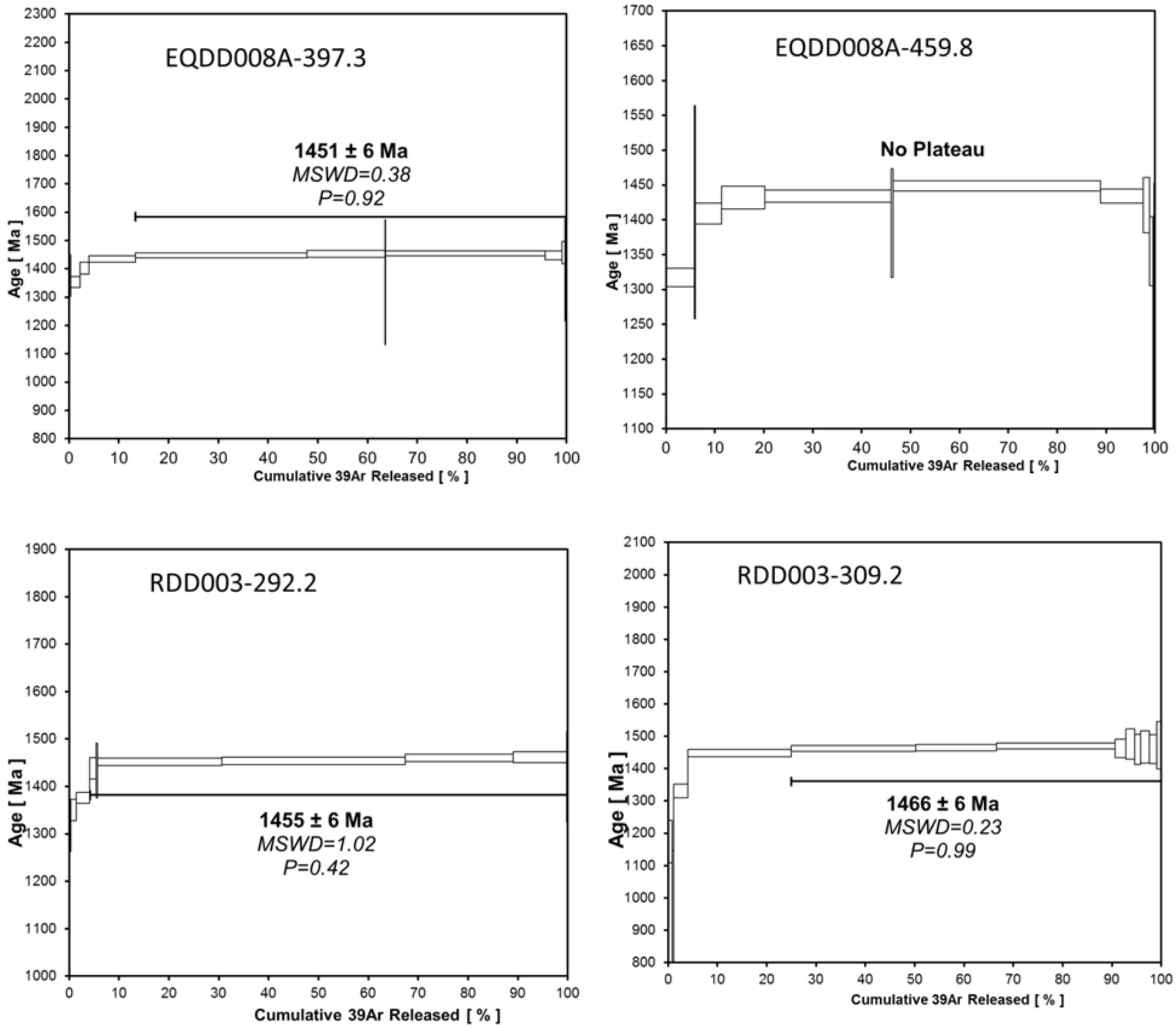

Figure 14 Biotite Ar/Ar geochronology results for EQDD008A-397.3, EQDD008A-459.8, RDD003-292.2 and RDD003-309.2. Location of Equis and Ranald drill holes shown in Figure 2.

DISCUSSION

Geochronological Interpretation

All geochronological results for this study are summarised in Table 6.

	Equis			Ranald				
	EQDD008A-397.3	EQDD008A-438.4	EQDD008A-459.8	RDD003-262	RDD003-267.3		RDD003-292.2	RDD003-309.2
Biotite Ar/Ar	1451 ± 6		No plateau				1455 ± 6	1466 ± 6
Monazite U-Pb	1518 ± 7	1500 ± 6	1495 ± 8	1533 ± 9	1544 ± 9	1477 ± 12	1509 ± 8	1489 ± 8
Zircon U-Pb							1538 ± 13	

Table 6 Summarised geochronological results from this study.

EQUIS

Monazite geochronology

Two age populations were obtained from monazite analysis of the three Equis samples; ca 1518 Ma and ~1498 Ma (Fig. 11). The ca 1498 Ma age is recognised from two samples, EQDD008A-438.4 (1500 ± 6 Ma) and EQDD008A-459.8 (1495 ± 8 Ma). The probability density curves from the EQDD008A samples are all symmetric bell shaped and show unimodal age data. The morphology and homogeneous zoning of the monazite grains suggest they are metamorphic in origin (Aleinikoff *et al.*, 2006). This suggests that the Equis region was affected by thermal activity at ca 1518 Ma and ca 1498 Ma. It is not possible to ascertain whether this was one continuous thermal event or two separate events.

Biotite geochronology

It is estimated that the closure temperature of Ar in biotite is 300 ^{O}C - 330 ^{O}C (McDougal and Harrison, 1999), which can be influenced by cooling rate, size and composition of the grains (Harrison *et al.*, 1985).

A cooling age of ca 1451 ± 6 Ma from sample EQDD008A-397.3 (Fig. 14: Table 6) was obtained, indicating the Equis area is cooled through the closure temperature of Ar within biotite (300 ^{O}C) at ca ~1450 Ma as suggested by the flat shape of the plateau (e.g. Harrison *et al.*, 1985).

The low temperature steps of this sample give a maximum age for a younger (minor) heating event at ~1350 - 1300 Ma.

Sample EQDD008A-459.8 did not record a plateau however the shape of the spectra indicates a similar history to sample EQDD008A-397.3. The biotite in sample EQDD008A-459.8 is partially to completely altered to chlorite and therefore a plateau was not attained.

RANALD

Zircon geochronology

U-Pb zircon geochronology yielded a single weighted age of 1538 ± 13 Ma (Fig. 10: Table 6).

The morphology of the zircon grains is round to sub round with many of the grains having an idioblastic shape with rounded terminations. The grain size is highly variable (50µm to 400µm). Hoskin and Black (2000) analysed metamorphic zircon grains that have similar morphology to the ones analysed in this study which indicate a metamorphic origin for the zircon grains from RDD003-292.2. It is accepted that Th/U ratios with a range of 0.1 to 0.9 from zircon grains indicate an igneous origin (e.g. Hoskin and Schaltegger, 2003). However, Goodge *et al.* (2001) records normal igneous zircon Th/U ratios (0.25 – 0.4) in metamorphic zircons found in eclogites in Antarctica. Therefore with no evidence of igneous zonation in the CL, the round to sub round morphology of the grains and the grains being clear in transmitted light it is suggested that the zircon grains analysed in this study are metamorphic in origin.

Monazite geochronology

Five age populations were yielded from monazite analysis of the four Ranald samples; ca ~1700 Ma, ca ~1600 Ma, ca ~ 1540 Ma, ca 1509 ± 8 Ma and ca ~1485 Ma (Fig. 12, Table 6). The ca 1485 Ma age is recognised from two samples, RDD003-267.3 (1477 ± 12 Ma) and RDD003-309.2 (1489 ± 8 Ma).

The ca 1540 Ma age is recognised from two samples, RDD003-262 (1533 ± 9 Ma) and RDD003-267.3 (1544 ± 9 Ma). The ca ~1600 Ma age is recognised as a small age population (total of 3 analyses) in samples RDD003-292.2 and RDD003-309.2.

The morphology and homogeneous zoning of the monazite grains suggest they are metamorphic in origin (Aleinikoff *et al.*, 2006). This suggests that the Ranald region was affected by thermal activity at ca 1540 Ma, ca 1509 Ma and ca 1485 Ma. The asymmetric shape found in the age probability density curves of the Ranald samples (Fig. 12) may represent continual monazite growth and/or resetting of monazite ages during metamorphism. However it is not possible to definitively determine whether thermal activity occurred as ne prolonged metamorphic event or as multiple discrete and closely spaced events during the period ca ~1580 Ma to ~ 1480 Ma.

The 1600 Ma and 1700 Ma ages obtained correspond to the Hiltaba and the Kimban events respectively. The limited data for these events indicate that whilst these widespread events may have affected the central Yorke Peninsula, they were either not as impactful on the central Yorke Peninsula as widely accepted or that the Hiltaba and Kimban events did affect the central Yorke Peninsula and later metamorphic event/s reset the U-Pb ages.

Biotite geochronology

Cooling ages of 1455 ± 6 Ma and 1466 ± 6 Ma from samples RDD003292.2 and RDD003-309.2 (Fig. 12: Table 6) were obtained. These ages are within error of each other and so are indistinguishable. The Ranald area is therefore suggested to have cooled through 300 ^{O}C at ca ~ 1460 Ma Ages as suggested by the flat shapes of the plateau ages (e.g. Harrison et al, 1995). The low temperature steps of RDD003-292.2 and RDD003-309.2 gives maximum ages for younger (minor) heating events at ~ 1350-1300 Ma and younger than 1150 Ma respectively.

Interpreted metamorphic conditions

EQUIS

The peak assemblage of the Equis area (Fig. 2) is fibrolitic sillimanite-quartz-microcline-plagioclase-biotite-magnetite-haematite. This assemblage has an estimated pressure-temperature (P-T) field of 650^{o}C to 800^{o}C and 4Kbars to 10Kbars (Fig. 6). This corresponds to an approximate geothermal gradient of 20-60 ^{o}C/Km (calculated assuming 1Kbar is a 3.5km thick sedimentary rock package) which is normal to elevated.

The observation of muscovite overprinting fibrolite in the peak assemblage of this sample allows the P-T path to be extended down temperature (Fig. 6). The P-T shape is restricted in its shape as it cannot start in the cordierite field due to no evidence of relic cordierite.

RANALD

The peak assemblage of sample RDD003-555.2 is fibrolite-microcline-quartz-biotite-plagioclase-magnetite-haematite with an estimated P-T field of 670^{o}C to 810^{o}C and

4Kbars to 10Kbars (Fig. 7). This corresponds to a normal to elevated geothermal gradient of 20 - 60 ^{o}C/Km.

Fibrolite in the peak assemblage is overprinted by cordierite (Fig. 5). This allows the P-T path to be drawn down pressure and temperature (Fig. 7) and indicates an initial down pressure path with minimal decrease in temperature followed by a rapid decrease in temperature with little pressure decrease.

Ca 1540 Ma to 1480 Ma thermal event

Metamorphic zircon from the Ranald drill hole (Fig. 2) yields an age of 1538 ± 13 Ma, which is within error of metamorphic monazite from samples RDD003-262 (1533 ± 9 Ma) and RDD003-267.3 (1544 ± 9 Ma). Numerous studies (e.g. Copeland *et al.*, 1988; Parrish, 1990) have demonstrated that metamorphic zircon grains commonly yield an older age than monazite grains from the same sample and metamorphic event due to different closure temperatures (e.g. Copeland *et al.*, 1988). However Kelsey *et al.* (2008) demonstrates that metamorphic zircon and monazite can yield similar ages due to the growth behaviour of the two minerals, and therefore in some cases it is possible they date the same thermal event. This has been demonstrated by Rubatto *et al.* (2001), who reported indistinguishable zircon and monazite U-Pb ages within a sample, giving strong evidence that the grains grew at the same point in the P-T evolution of the rock. Here, we suggest that the indistinguishable zircon and monazite ages from the Ranald drill hole date the same thermal event at ~ ca 1540 Ma. The new monazite and zircon U-Pb geochronological data presented in this study shows the central Yorke Peninsula was affected by thermal activity at ca 1540 to 1480 Ma. It is unknown whether thermal activity constituted multiple events, or was a single protracted event. It is suggested the Ranald monazite grains may have been continually forming over this prolonged period instead of growth being initiated during a restricted time due to the asymmetric nature of the U-Pb probability curves (Fig. 12). Whereas the probability density curves for the Equis samples have symmetric bell shapes which suggest that monazite growth initiated at similar P-T conditions as each other before being exhumed.

There is limited data on thermal activity in the Gawler Craton during ~1540 – 1480 Ma. A high-temperature event has been described for the northern Gawler Craton at ca 1550 – 1530 Ma (Hand et al., 2007). The thermal evolution associated with this event is unknown (Hand et al., 2007). Magmatism during 1540 – 1480 Ma is recognised by the 1497 ± 13 Ma Spilsby granites on Spilsby Island offshore of Eyre Peninsula (Fanning, 1997; Fig. 1) and A-type magmatism in the Coompana region (Fig. 1) at 1505 ± 7 Ma (Wade *et al.*, 2007). The mechanism for this thermal pulse and magmatic activity in the Coompana region is unknown (Wade *et al.*, 2007).

On the Yorke Peninsula, the period 1540 - 1480 Ma is characterised by high temperatures, moderate pressures and normal to elevated geothermal gradients (Figs 11 and 12). Elevated geothermal gradients are generally suggested to be the result of (a) sill like igneous intrusion at intermediate crustal levels (e.g. Lux *et al.*, 1986); (b) increased crustal heating as a result of intrusion of magmas beneath or into a given terrain (e.g. Bohlen, 1987) and (c) anomalously high mantle heat flow due to rifting (e.g. Wickham and Oxburgh, 1985).

The emplacement of voluminous granitoid bodies as the only possible driver of this thermal event is not possible on the Yorke Peninsula. There is magmatism such as the emplacement of the Spilsby Granite, the magmatism in the Coompana Block and the undated granites under cover on the Yorke Peninsula (figure 2 in Conor *et al.*, 2010). Zang et al. (2007) suggests that the intrusion of the Spilsby granites provided the heat source for age resetting at ~1500 Ma in the northern Yorke Peninsula area. However, Barton and Hanson (1989) and Collins and Vernon (1991) demonstrate that the volume of granites needed to create a thermal event large enough to regionally reset metamorphic ages is large (>50% of total rock volume). You would also need magmatism to be active for the entirety of the thermal event. With limited evidence for 1500 Ma magmatism it is very unlikely that the Spilsby granites and the A-type magmatism in the Coompana region are voluminous or long lived enough to supply the amount of heat needed to create an elevated geothermal gradient for the duration of the 1540 – 1480 Ma thermal event. The undated granites on the Yorke Peninsula are widely suggested to be of Hiltaba event age (figure 2 in Conor *et al.*, 2010) which is ~ 50 Ma before the thermal event on the Yorke Peninsula and therefore unlikely to contribute to the thermal event. It is likely that while the 1500 Ma magmatism was not the sole mechanism for the thermal event, it could have contributed to it.

Another possible cause of the high geothermal gradient in the Gawler Craton is extension. The western Gawler Craton during 1550 – 1450 Ma was characterised by major reactivation of craton-scale faults and shear zones (Swain *et al.*, 2005; Fraser and Lyons, 2006). This reactivation of major structures may be evidence of extension. However there is too little data to conclusively suggest extension as the principal tectonothermal driver during 1540 – 1480 Ma.

Thomas *et al.* (2008) obtained peak metamorphic ages of 1557 ± 15 Ma from the Fowler Domain in the northern Gawler Craton, which is similar to 1543 ± 9 Ma metamorphic age Daly *et al.* (1998) recorded from metamorphic zircon grains in a mafic granulite. Currently there is minimal evidence that 1540 – 1480 Ma thermal activity in the Yorke Peninsula is related to the 1550 - 1530 Ma event in the northern Gawler Craton. It is however, possible that magmatism in the southern Gawler Craton and deformation and high-temperature metamorphism (Hand *et al.*, 2007) in the northern Gawler Craton is linked.

Thermal activity in the central Yorke Peninsula is ~ 50 Ma younger than the Hiltaba Event. The Hiltaba Event is extensive in the Gawler Craton (e.g. Conor, 2002) and the Moonta-Wallaroo region (Conor *et al.*, 2010); however with the exception of three U-Pb metamorphic monazite ages (this study) there is minimal evidence of ca 1600 - 1570 Ma Hiltaba activity (magmatism, deformation, metamorphism and mineralisation) seen on the central Yorke Peninsula. The minimal evidence indicates that whilst the Hiltaba event may have affected the central Yorke Peninsula to some degree, it may have not been as intense as in other areas of the craton or, evidence of the event has been obscured by the younger ca 1540 – 1480 Ma thermal activity and resetting of monazite and zircon U-Pb ages. Assessment of the intensity of deformation and metamorphism on the Yorke Peninsula during the Hiltaba Event is also hindered by the limited availability of the data on the region.

Exhumation history

Biotite Ar/Ar ages give cooling to ~300^{o}C (Harrison *et al.*, 1995) at ca. 1450 Ma (Equis) and ~ 1460 Ma (Ranald). Cooling rates were calculated for Equis and Ranald regions by combining the peak metamorphic conditions, the biotite Ar/Ar ages and the U-Pb ages calculated in this study. Cooling rates of ~ 4^{o}C/Ma – 10^{o}C/Ma for the Equis sample area (Fig. 15) and a range of ~ 4^{o}C/Ma – 25^{o}C/Ma (Fig. 15) in the Ranald area were obtained. These cooling rates suggest that the central Yorke Peninsula underwent an 'active' cooling history (Stüwe and Ehlers, 1998; Forbes *et al.*, 2012) compared to a 'passive' cooling history (e.g. cooling due to the termination of a heat source such as an igneous intrusion: Forbes *et al.*, 2012). This implies cooling was associated with exhumation due to tectonic activity (Stüwe and Ehlers, 1998; Forbes *et al.*, 2012). Betts *et al.* (2002) and Betts and Giles (2006) suggest lithospheric extension occurred in the Australian Continent during ca 1470 – 1450 Ma. This theory is supported by: The remnants of the ca 1450 Ma Cariewerloo intracontinental basin (Fanning *et al.*, 1983) with the deposition of the ca 1420 Ma Pandurra formation (Webb *et al.*, 1986); rapid cooling at ~ 1425 Ma on the south-eastern Eyre Peninsula (Foster and Ehlers, 1998) and biotite and muscovite Ar/Ar geochronology ages of ~ 1440 Ma within the Karari shear zone and the Tallacootra shear zone in the north-western Gawler Craton (Fraser and Lyons, 2006). During the ca 1500 – 1450 Ma period two tectonothermal events are recognised in the Gawler Craton: The Wartaken event (Brittle faulting and regional folding: Parker and Lemon, 1982; Fanning *et al.*, 1988) and the Coorabie event (reactivation of shear zones at greenschist to amphibolite facies and regional cooling: Direen *et al.*, 2005; Hand *et al.*, 2007). While the tectonic drivers of these events are unclear (Direen *et al.*, 2005; Swain *et al.*, 2005; Hand *et al.*, 2007) Hand *et al.* (2007) suggests that reactivation of shear zones at this time could have been associated with regional denudation of the Gawler Craton. Exhumation in the Fowlers Domain in the western Gawler Craton (Fig. 1) was accommodated by major structures during 1470 to 1450 Ma (Thomas *et al.*, 2008). In the central Yorke Peninsula exhumation during 1500 – 1450 Ma may have been accommodated by the Pine Point Fault (a major long-lived structure that runs N-S along the eastern coast of the Yorke Peninsula and is proximal to the Equis and Ranald areas: Fig. 2).

It is possible that extension and exhumation during ca 1470 – 1450 Ma (e.g. Betts *et al.*, 2002) and its associated reactivation of major structures (Direen *et al.*, 2005) was accommodated by the Pine Point Fault and other major faults on the Yorke Peninsula.

In the Ranald area the shape of the P-T path (Fig. 7) shows an initial drop in pressure faster than temperature. After this initial stage, the path is interpreted to drop in temperature faster relative to the drop in pressure. This suggests the region was being exhumed while still hot, and therefore exhumation initiated before the cessation of the 1540 to 1480 Ma thermal activity. Conversely, the Equis area shows a P-T path (Fig. 6) with temperature and pressure decreasing at similar rates. These differences between the two paths suggest movement and exhumation along the Pine Point Fault is not homogeneous in terms of accommodation of deformation and strain rates.

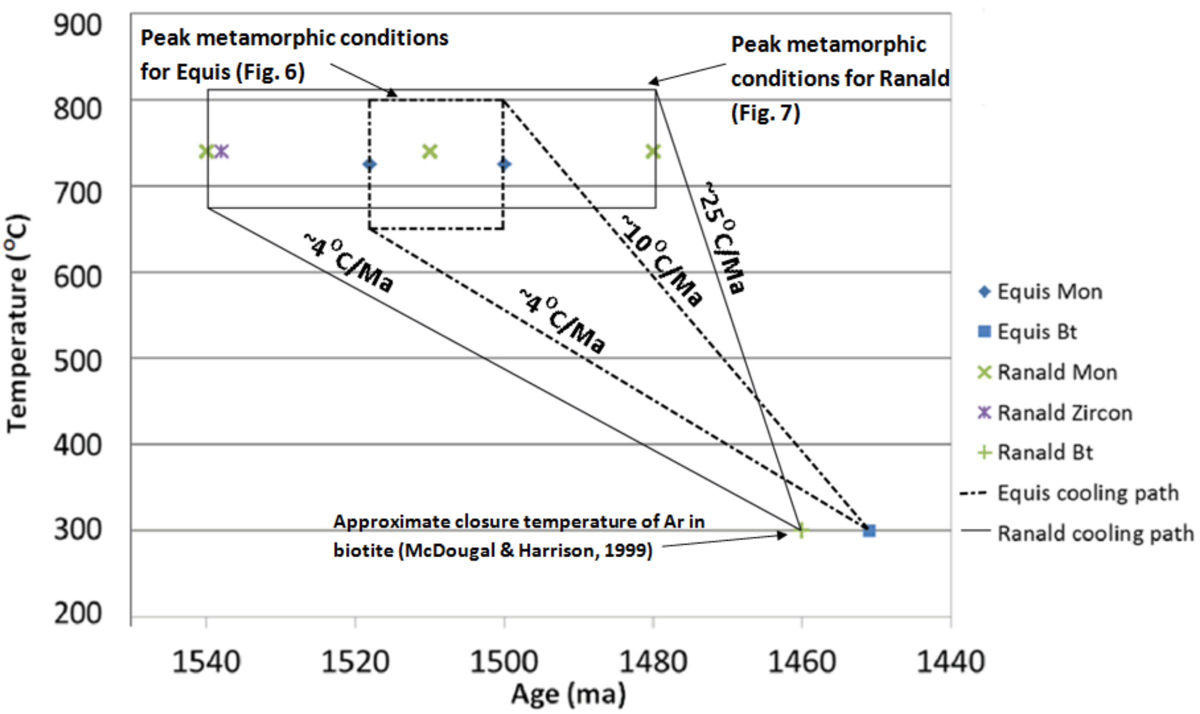

Figure 15 Schematic diagram showing age versus temperature for the Equis and Ranald areas.

Implications on mineralisation

Mineralisation in the Gawler Craton (e.g. Moonta-Wallaroo, Punt Hill and Olympic Dam) is related to the Hiltaba event (e.g. Johnson and Cross, 1995; Reid *et al.*, 2011). Alteration associated with mineralisation in the Hillside deposit (Fig. 1) has been dated at ca 1570 ± 8 Ma (Conor *et al.*, 2010) and is therefore also related to mineralisation in the Gawler Craton during the Hiltaba Event. Metamorphism occurred during ca 1540 – 1480 Ma in the area proximal to the Hillside deposit and could have been one prolonged pulse of thermal activity or multiple discrete thermal events. Mineralisation on the central Yorke Peninsula is ~50 Ma older than peak metamorphism. It is therefore conceivable that mineralisation was affected by this later peak metamorphic event/s. Metamorphic grade on the Yorke Peninsula varies from amphibolite to granulite facies in the central region (this study) to amphibolite to greenschist facies in the Moonta-Wallaroo region (Conor, 2002). Brittle faults and structures are prominent in the Moonta-Wallaroo region (Conor, 2002) which could be a result of deformation during greenschist-amphibolite grade metamorphism. With the amphibolite to granulite facies around the Hillside deposit it is therefore conceivable that metamorphism affected mineralisation in a ductile/shear fabric in such ways as redistributing, concentration and remobilisation.

Possible Hiltaba-age mineralisation situated along the Pine Point Fault (e.g. Hillside; Fig. 2) would be affected by extension, exhumation and the reactivation of craton-scale structures during ca 1500 – 1450 Ma. Movement along the Pine Point Fault would possibly redistribute mineralisation along this long-lived major structure. The reduction of pressure may also have helped mineralisation to form or be trapped in structures such as dilational jogs along the Pine Point Fault. It is therefore recommended future exploration focus on The Pine Point Fault and decompressional structures along the Pine Point Fault such as dilational jogs.

CONCLUSION

During ca 1540 – 1480 Ma one prolonged thermal event or multiple thermal events affected the region around Hillside on the Yorke Peninsula. The peak pressure-temperature conditions for this event was 4-10 Kbars and ~650 to 810^{O} C, corresponding to normal to elevated geothermal gradient of 20 – 60 ^{O} C/Km. The tectonothermal driver for metamorphism is unclear but may have been due to a combination of extension and igneous intrusion. Metasediments cooled past ~300 ^{O}C at approximately 1450 Ma as interpreted from the biotite Ar/Ar geochronology results. This is comparable to the Eyre Peninsula during the Wartaken Event and the north-western Gawler Craton during the Coorabie Orogeny. It is suggested that lithospheric extension occurred in the Australian Continent during ca 1470 – 1450 Ma and this may be seen in the Gawler Craton in terms of the reactivation of shear zones and structures, basin formation and brittle faulting. On the Yorke Peninsula this extension, reactivation of shear zones and exhumation was possibly accommodated along the Pine Point Fault. Mineralisation of the Hillside deposit on the central Yorke Peninsula is understood to be temporally associated with 1600 – 1570 Ma Hiltaba-age IOCG mineralisation in the Gawler Craton. Peak metamorphism is suggested to have occurred on the central Yorke Peninsula at ca 1540 – 1480 Ma which is ~ 50 Ma later than mineralisation. Given the proximity of the Hillside deposit and the sample areas, it can be proposed that mineralisation at the Hillside deposit (and other possible undiscovered Hiltaba-age mineralised deposits) were deformed and metamorphosed during the 1540 – 1480 Ma thermal event. Hiltaba-age mineralisation may also have been affected by the 1500 – 1450 Ma extensional events in the form of redistribution, concentration and remobilization along the Pine Point Fault.

ACKNOWLEDGMENTS

The author would like to thank Dr Caroline Forbes from the University of Adelaide for her enthusiastic and patient mentoring as Supervisor for this project and Dr Dave Giles as secondary supervisor.

Generous financial support was provided by Rex Minerals. Marc Twining and Patrick Say have been invaluable for their knowledge of the project area and interest in the project.

Graham Teale, Mark Fanning and Colin Conor are whole heartedly thanked for selflessly giving up their free time and endless knowledge in topics such as Gawler Craton, geochronology and petrology.

From Adelaide Microscopy many thanks go to Benjamin Wade for his expertise in U-Pb geochronology, EPMA software and patience in answering general queries.

I would also like to thank Jade Anderson and Laura Morrissey for their diligent help with Thermocalc and creating the P-T diagrams.

REFERENCES

Aleinikoff, J.N., Schenck, W.S., Plank, M.O., Srogi, L., Fanning, C.M., Kamo, S.L. and & Bosbyshell, H., 2006. Deciphering Igneous and Metamorphic Events in High-Grade Rocks of the Wilmington Complex, Delaware: Morphology, Cathodoluminescence and Backscattered Electron Zoning, and Shrimp U-Pb Geochronology of Zircon and Monazite. Geological Society of America Bulletin, 118(1-2): 39-64.

Betts, P.G. and Giles, D., 2006. The 1800–1100 Ma Tectonic Evolution of Australia. Precambrian Research, 144(1–2): 92-125. Betts, P.G., Giles, D., Lister, G.S. and Frick, L.R., 2002. Evolution of the Australian Lithosphere. Australian Journal of Earth Sciences, 49(4): 661-695.

Bohlen, S.R., 1987. Pressure-Temperature-Time Paths and a Tectonic Model for the Evolution of Granulites. The Journal of Geology, 95(5): 617-632.

Conor, C., 1995. Moonta-Wallaroo Region: An Interpretation of the Geology of the Maitland and Wallaroo 1: 100 000 Sheet Areas. Mines and Energy South Australia, Open File Envelope, 8886.

Conor, C., 2002. The Palaeo-Mesoproterozoic Geology of Northern Yorke Peninsula, South Australia; Hiltaba Suite-Related Alteration and Mineralisation of the Moonta-Wallaroo Cu-Au District: Department of Primary Industries and Resources South Australia. Adelaide, South Australia, Australia.

Conor, C., Raymond, O.L., Baker, T., Teale, G., Say, P. and Lowe, G., 2010. Alteration and Mineralisation in the Moonta-Wallaroo Copper-Gold Mining Field Region, Olympic Domain, South Australia. PGC Publishing, Adelaide.

Copeland, P., Parrish, R.R. and Harrison, T.M., 1988. Identification of Inherited Radiogenic Pb in Monazite and Its Implications for U-Pb Systematics. Nature, 333(6175): 760-763.

Cowley, W., Conor, C. and Zang, W., 2003. New and Revised Proterozoic Stratigraphic Units on Northern Yorke Peninsula. MESA Journal, 29: 46-58.

Daly, S., Fanning, G. and Fairclough, M., 1998. Tectonic Evolution and Exploration Potential of the Gawler Craton, South Australia. AGSO Journal of Australian Geology and Geophysics, 17: 145-168.

Direen, N.G., Cadd, A.G., Lyons, P. and Teasdale, J.P., 2005. Architecture of Proterozoic Shear Zones in the Christie Domain, Western Gawler Craton, Australia: Geophysical Appraisal of a Poorly Exposed Orogenic Terrane. Precambrian Research, 142(1–2): 28-44.

Fanning, C., 1997. Geochronological Synthesis of Southern Australia. Part II. The Gawler craton. PRISE—Precision radiogenic isotope services report: Canberra, Australia, Australian National University, and South Australia, Department for Primary Industries and Resources, Open File Envelope, 8918: 1-45.

Fanning, C., Flint, R. and Preiss, W., 1983. Geochronology of the Pandurra Formation: South Australia Geological Survey Quarterly Geology Notes, V. 88.

Fanning, C.M., Flint, R.B., Parker, A.J., Ludwig, K.R. and Blissett, A.H., 1988. Refined Proterozoic Evolution of the Gawler Craton, South Australia, through U-Pb Zircon Geochronology. Precambrian Research, 40–41(0): 363-386.
Forbes, C.J., Giles, D., Jourdan, F., Sato, K., Omori, S. and Bunch, M., 2012. Cooling and Exhumation History of the Northeastern Gawler Craton, South Australia. Precambrian Research, 200–203(0): 209-238.
Foster, D.A. and Ehlers, K., 1998. 40ar-39ar Thermochronology of the Southern Gawler Craton, Australia: Implications for Mesoproterozoic and Neoproterozoic Tectonics of East Gondwana and Rodinia. Journal of Geophysical Research B: Solid Earth, 103(5): 10177-10193.
Fraser, G.L. and Lyons, P., 2006. Timing of Mesoproterozoic Tectonic Activity in the Northwestern Gawler Craton Constrained by 40ar/39ar Geochronology. Precambrian Research, 151(3–4): 160-184.
Goodge, J.W., Fanning, C.M. and Bennett, V.C., 2001. U–Pb Evidence of ~1.7 Ga Crustal Tectonism During the Nimrod Orogeny in the Transantarctic Mountains, Antarctica: Implications for Proterozoic Plate Reconstructions. Precambrian Research, 112(3–4): 261-288.
Hand, M., Reid, A. and Jagodzinski, L., 2007. Tectonic Framework and Evolution of the Gawler Craton, Southern Australia. Economic Geology, 102(8): 1377-1395. Available from <Go to ISI>://WOS:000254227400002.
Harrison, T.M., Duncan, I. and McDougall, I., 1985. Diffusion of 40ar in Biotite: Temperature, Pressure and Compositional Effects. Geochimica et Cosmochimica Acta, 49(11): 2461-2468.
Hoek, J.D. and Schaefer, B.F., 1998. Palaeoproterozoic Kimban Mobile Belt, Eyre Peninsula: Timing and Significance of Felsic and Mafic Magmatism and Deformation. Australian Journal of Earth Sciences, 45(2): 305-313.
Hoskin, P. and Black, L., 2000. Metamorphic Zircon Formation by Solid-State Recrystallization of Protolith Igneous Zircon. Journal of Metamorphic Geology, 18(4): 423-439.
Hoskin, P.W. and Schaltegger, U., 2003. The Composition of Zircon and Igneous and Metamorphic Petrogenesis. Reviews in mineralogy and geochemistry, 53(1): 27-62.
Jackson, S.E., Pearson, J.J., Griffen, W.L.,and Belousova, E.A., 2004, The application of Laser ablation-inductively coupled plasma-mass spectrometry to in situ U-Pb zircon geochronology: Chemical Geology, v. 211, p.47-69.
Johnson, J.P. and Cross, K.C., 1995. U-Pb Geochronological Constraints on the Genesis of the Olympic Dam Cu-U-Au-Ag Deposit, South Australia. Economic Geology, 90(5): 1046-1063.
Jourdan, F., And Renne, P.R.., 2007 Age calibration of the Fish Canyon sanindine 40Ar/39Ar dating standard using primary K-Ar standards: Geochemica et Cosmochimica Acta, v 71, p. 387-402.
Kelsey, D.E., Clark, C. and Hand, M., 2008. Thermobarometric Modelling of Zircon and Monazite Growth in Melt-Bearing Systems: Examples Using Model Metapelitic and Metapsammitic Granulites. Journal of Metamorphic Geology, 26(2): 199-212.

Koopers, A.A.P., 2002, ArArCalc-software for 40Ar/39Ar age calculations: computers& Geosciences, v. 28, p. 605-619.
Kretz, R., 1983. Symbols for Rock-Forming Mineralsl. American mineralogist, 68: 277-279.
Lee, D., Severn, G., Oksuz, L., Hershkowitz, N., 2006. Laser-inducedfluorescence measurements of argon ion velocities near the sheath boundary of an argon-xenon plasma. Journal of Physics: Applied Physics v. 39, number 24, 5230
Lux, D.R., DeYoreo, J.J., Guldotti, C.V. and Decker, E.R., 1986. Role of Plutonism in Low-Pressure Metamorphic Belt Formation. Nature, 323(6091): 794-797.
McDougal, I. and Harrison, T.M., 1999. Geochronology and Thermochronology by the 40ar/39ar Method. Oxford University Press, Oxford.
Parker, A.J. and Lemon, N.M., 1982. Reconstruction of the Early Proterozoic Stratigraphy of the Gawler Craton, South Australia. Journal of the Geological Society of Australia, 29(1-2): 221-238.
Parrish, R.R., 1990. U-Pb Dating of Monazite and Its Application to Geological Problems. Canadian Journal of Earth Sciences, 27(11): 1431-1450.
Pollard, P.J., 2006. An Intrusion-Related Origin for Cu–Au Mineralization in Iron Oxide–Copper–Gold (Iocg) Provinces. Mineralium Deposita, 41(2): 179-187.
Reid, A., Swain, G., Mason, D. and Maas, R., 2011. Punt Hill Iocg Project, Eastern Gawler Craton: Nature and Timing of Iocg Mineralisation. MESA Journal, 60: 7-17.
Renne, P.R, Mundil, R, Balco, G., Min, K., Ludwig, K.R., 2010. Joint determination of 40K decay constraints and 40Ar/40K for the Fish Canyon Sanindine Standard, and improved accuracyfor 40Ar/39Ar geochronology. Geochim Cosmochim. Acta 74, 5349-5367pp.
Rubatto, D., Williams, I.S. and Buick, I.S., 2001. Zircon and Monazite Response to Prograde Metamorphism in the Reynolds Range, Central Australia. Contributions to Mineralogy and Petrology, 140(4): 458-468.
Skirrow, R.G., Bastrakov, E.N., Barovich, K., Fraser, G.L., Creaser, R.A., Fanning, C.M., Raymond, O.L. and Davidson, G.J., 2007. Timing of Iron Oxide Cu-Au-(U) Hydrothermal Activity and Nd Isotope Constraints on Metal Sources in the Gawler Craton, South Australia. Economic Geology, 102(8): 1441-1470.
Stüwe, K. and Ehlers, K., 1998. Distinguishing Cooling Histories Using Thermometry. Interpretations of Cooling Curves with Some Examples from the Glein-Koralm Region and the Central Swiss Alps. Mitteilungen. österreichische Geologische Gesellschaft, 89: 201-212.
Swain, G.M., Hand, M., Teasdale, J., Rutherford, L. and Clark, C., 2005. Age Constraints on Terrane-Scale Shear Zones in the Gawler Craton, Southern Australia. Precambrian Research, 139(3–4): 164-180.
Thomas, J.L., Direen, N.G. and Hand, M., 2008. Blind Orogen: Integrated Appraisal of Multiple Episodes of Mesoproterozoic Deformation and Reworking in the Fowler Domain, Western Gawler Craton, Australia. Precambrian Research, 166(1): 263-282.

Wade, B.P., Payne, J.L., Hand, M. and Barovich, K.M., 2007. Petrogenesis of Ca 1.50 Ga Granitic Gneiss of the Coompana Block: Filling the 'Magmatic Gap'of Mesoproterozoic Australia. Australian Journal of Earth Sciences, 54(8): 1089-1102.

Webb, A.W., Thomson, B.P., Blissett, A.H., Daly, S.J., Flint, R.B. and Parker, A.J., 1986. Geochronology of the Gawler Craton, South Australia. Australian Journal of Earth Sciences, 33(2): 119-143.

Wickham, S.M. and Oxburgh, E.R., 1985. Continental Rifts as a Setting for Regional Metamorphism. Nature, 318(6044): 330-333.

APPENDIX A: ANALYTICAL TECHNIGUE FOR SEPERATION OF MONAZITE AND ZIRCON GRAINS AND U-Pb DATING

U-Pb monazite geochronology was undertaken via Laser Ablation Inductively Coupled Plasma Mass Spectrometry (LA-ICP-MS) at Adelaide Microscopy, University of Adelaide, Australia following Payne *et al.* (2008). U–Pb isotopic analyses were obtained using a New Wave 213 nm Nd-YAG laser in a He ablation atmosphere, coupled to an Agilent 7500cs ICP-MS. A 40s gas blank was analysed followed by 60s of measurement during zircon and monazite ablation, this is done to assure background readings are consistent and low. The laser was fired for 10s with the shutter closed to allow beam stabilisation prior to each ablation. The beam diameter was 20 μm for monazite analysis and 30 μm for the zircon analysis. A laser frequency of 5 Hz and output laser percentage of 55% resulted in an average fluence of 7 J/cm2 at the ablation site.

Isotopes measured for the study of monazite grains were 204Pb, 206Pb, 207Pb and 238U for 10, 15, 30 and 15 milliseconds respectively. Isotopes measured for zircon analysis were 204Pb, 206Pb, 207Pb, 208Pb, 232U and 238U with dwell times of 10, 15, 30, 10, 10 and 15 milliseconds respectively. U–Pb fractionation was corrected using the MAdel Monazite standard of age 492.01 ± 0.77 Ma and GEMOC GJ-1 zircon standard of age of 607.7 ± 4.3Ma (Jackson *et al.*, 2004). The real-time correction program 'Glitter' developed at Macquarie University, Sydney (Jackson *et al.*, 2004) was used for age corrections.

APPENDIX B: AR/AR SAMPLE PREPARATION AND ANALYTICAL TECHNIQUE

Optically transparent, ~600 × 400 μm-size biotite grains were handpicked under a binocular microscope. The grains were leached in diluted hydrofluoric acid for one minute and rinsed thoroughly with distilled water in an ultrasonic cleaner. Samples were loaded into two large wells (a 1.9 cm diameter and a 0.3 cm deep aluminium disc). These wells were bracketed by small wells that included Fish Canyon sanidine (FCs) used as a neutron fluence monitor for which an age of 99.738 ± 0.100 Ma (1σ) was adopted (Renne *et al.*, 2010) based on the calibration by Jourdan and Renne (2007). The wells were Cd-shielded to minimize undesirable nuclear interference reactions, and irradiated for 40 hours in the Hamilton McMaster University nuclear reactor (Canada) in position 5C.

The mean J-values computed from standard grains within the small pits are 0.00848400 ± 0.00001612. This was determined as the average and standard deviation of J-values of the small wells for each irradiation disc. Mass discrimination was checked using an automated air pipette and provided a mean value of 1.006302 ± 0.34 (34 %) per dalton (atomic mass unit) relative to an air ratio of 298.56 ± 0.31 (Lee *et al.*, 2006). Correction factors used for interfering isotopes were (39Ar/37Ar) Ca = 7.06 x10-4 (± 10 %), (36Ar/37Ar) Ca = 2.81x10-4 (± 3 %) and (40Ar/39Ar) K = 6.76x10-4 (± 10 %). The 40Ar/39Ar analyses were performed at the Western Australian Argon Isotope Facility at Curtin University.

Using a 110 W spectron Laser Systems the samples were step-heated. A continuous Nd-YAG (IR; 1064 nm) laser rastered over the sample for a 1 minute period to ensure a homogenously distributed temperature. In a stainless steel extraction line the gas was purified using three SAES AP10 getters and a liquid nitrogen condensation trap. Ar isotopes were measured in static mode using a MAP 215-50 mass spectrometer with a resolution of ~500 and a sensitivity of 4x10-14 mol/V. The MAP 215-50 was fitted with a Balzers SEV 217 electron multiplier mostly using 9 to 10 cycles of peak-hopping.

Data acquisition was done with the Argus program written by M.O. McWilliams. The raw data were processed using the ArArCALC software (Koppers, 2002) and ages calculated using the decay constants recommended by Renne *et al.* (2010). Blanks were monitored every 3 to 4 steps with typical 40Ar blanks ranging from 1 x 10-16 to 2 x 10-16 mol. Determining plateaus according to the following Criteria: plateaus must include at least 70 % of 39Ar. The plateau should be distributed over a minimum of 3 consecutive steps consistent at 95 % confidence level and satisfying a probability of fit (P) of at least 0.05. Plateau ages (Fig. 14) are given at the 2σ level and are calculated using the mean of all the plateau steps, each weighted by the inverse variance of their individual analytical error. Mini-plateaus are likewise defined with the exception that they include between 50 % and 70 % of 39Ar. Integrated ages (2σ) are calculated using the total gas released for each Ar isotope. Inverse isochrons include the maximum number of steps with a probability of fit ≥ 0.05. Uncertainties are included in the calculation.

APPENDIX C: ZIRCON ANALYSIS RESULTS TABLE

Spot number	U (ppm)	Th (ppm)	Th/U	^{204}Pb	^{206}Pb	Radiogenic Ratios $^{206}Pb/^{238}U$	±	$^{207}Pb/^{235}U$	±	$^{207}Pb/^{206}Pb$	±	Age (Ma) $^{207}Pb/^{206}Pb$	±	$^{206}Pb/^{238}U$	±
Z1	2875	2626	0.91	82	1716459	0.259	0.0039	3.334	0.0502	0.094	0.0010	1500.4	20.03	1482.5	19.81
Z2	1635	1359	0.83	142	940368	0.254	0.0038	3.366	0.0509	0.096	0.0010	1553.3	20.05	1458.2	19.57
Z3	2362	1605	0.68	54	1275720	0.243	0.0037	3.219	0.0489	0.096	0.0010	1553.1	20.12	1401.4	18.92
Z4	3055	1668	0.54	143	1647616	0.247	0.0037	3.179	0.0485	0.093	0.0010	1495.5	20.37	1424.3	19.23
Z5	2150	1171	0.54	25	1120619	0.244	0.0037	3.131	0.0480	0.093	0.0010	1493.9	20.54	1405.8	19.05
Z6	4089	1547	0.38	3	2087436	0.243	0.0037	3.130	0.0482	0.093	0.0010	1495.2	20.63	1404.4	19.07
Z7	1850	1589	0.85	61	900727	0.237	0.0036	2.989	0.0465	0.092	0.0010	1462.5	21.15	1368.6	18.67
Z8	3044	1402	0.46	49	1517204	0.248	0.0038	3.185	0.0495	0.093	0.0010	1496.7	20.94	1425.8	19.42
Z9	4860	1425	0.29	34	2405147	0.251	0.0038	3.189	0.0499	0.092	0.0010	1472.7	21.27	1443.6	19.68
Z10	2239	1469	0.65	44	1079189	0.250	0.0038	3.243	0.0511	0.094	0.0011	1513.8	21.27	1437.3	19.65
Z11	2259	1362	0.60	28	1071663	0.251	0.0038	3.281	0.0520	0.095	0.0011	1526	21.45	1444.1	19.78
Z12	2277	1436	0.63	0	181202	0.273	0.0041	3.658	0.0646	0.097	0.0014	1569.9	27.24	1557	20.78
Z13	2159	1206	0.56	0	162064	0.261	0.0039	3.497	0.0624	0.097	0.0015	1573.1	27.64	1493.5	20.06
Z14	1824	1198	0.65	0	137749	0.265	0.0040	3.535	0.0638	0.097	0.0015	1560.8	28.19	1516.8	20.38
Z15	2150	881	0.41	1	154200	0.255	0.0039	3.445	0.0627	0.098	0.0015	1587.1	28.45	1463.7	19.77
Z16	4620	2828	0.61	0	329959	0.257	0.0039	3.471	0.0635	0.098	0.0015	1587.4	28.65	1473.5	19.89
Z17	2487	1300	0.52	1	178175	0.261	0.0040	3.481	0.0647	0.097	0.0015	1563.9	29.45	1493.7	20.21
Z18	3874	1625	0.42	3	269104	0.255	0.0039	3.395	0.0631	0.096	0.0015	1557.3	29.53	1465.5	19.82
Z19	3730	1616	0.43	13	253976	0.252	0.0038	3.386	0.0621	0.098	0.0015	1578.8	29.06	1447.3	19.46
Z20	3207	1210	0.37	2	224980	0.265	0.0040	3.583	0.0690	0.098	0.0016	1589.1	30.95	1514.4	20.59
Z21	1731	1264	0.72	8	119781	0.264	0.0041	3.553	0.0698	0.097	0.0017	1576.4	31.91	1512.5	20.67
Z22	2765	2127	0.76	5	186941	0.262	0.0040	3.467	0.0687	0.096	0.0017	1550	32.44	1498.4	20.52
Z23	1657	1261	0.75	7	107308	0.254	0.0039	3.438	0.0695	0.098	0.0018	1590.7	33.2	1458.4	20.14
Z24	2644	1290	0.48	12	176755	0.265	0.0041	3.561	0.0727	0.097	0.0018	1573.1	33.71	1517.9	20.89
Z25	1859	1227	0.66	8	131880	0.282	0.0043	3.696	0.0668	0.095	0.0015	1527.6	28.46	1603	21.47
Z26	2323	1390	0.60	0	156502	0.268	0.0041	3.545	0.0648	0.096	0.0015	1544.2	28.88	1532.5	20.68
Z27	4322	618	0.14	8	270932	0.250	0.0038	3.203	0.0592	0.093	0.0015	1483.7	29.67	1440.3	19.63
Z28	2241	890	0.40	11	142063	0.253	0.0039	3.230	0.0609	0.093	0.0015	1478.8	30.61	1454.7	19.88
Z29	1610	1190	0.74	12	108843	0.267	0.0041	3.493	0.0667	0.095	0.0016	1523.9	31.19	1526.9	20.64
Z30	2332	966	0.41	0	155177	0.265	0.0041	3.564	0.0692	0.097	0.0017	1574.5	31.52	1517.8	20.73
Z31	2409	964	0.40	11	158910	0.262	0.0040	3.499	0.0691	0.097	0.0017	1561	32.38	1502.6	20.56
Z32	1880	823	0.44	10	122633	0.261	0.0040	3.472	0.0701	0.097	0.0017	1560.7	33.35	1492.7	20.59
Z33	2170	890	0.41	10	140017	0.257	0.0040	3.417	0.0700	0.096	0.0018	1552.8	34.13	1476.8	20.44
Z34	2173	1103	0.51	0	151645	0.278	0.0043	3.700	0.0771	0.096	0.0018	1557	34.94	1582.3	21.78
Z35	1816	1268	0.70	12	119932	0.263	0.0041	3.465	0.0738	0.095	0.0019	1537	36.05	1506.9	20.96

APPENDIX C: ZIRCON ANALYSIS RESULTS TABLE - CONTINUED

						Radiogenic Ratios						Age (Ma)			
Spot number	U (ppm)	Th (ppm)	Th/U	^{204}Pb	^{206}Pb	$^{206}Pb/^{238}U$	±	$^{207}Pb/^{235}U$	±	$^{207}Pb/^{206}Pb$	±	$^{207}Pb/^{206}Pb$	±	$^{206}Pb/^{238}U$	±
Z36	4639	50788	10.9	10	289088	0.249	0.0039	3.258	0.0705	0.095	0.0019	1524.5	36.83	1434.2	20.13
Z37	2768	1189	0.43	0	185494	0.267	0.0040	3.510	0.0620	0.095	0.0014	1536.7	27.76	1524.8	20.44
Z38	2711	912	0.34	8	177675	0.261	0.0040	3.359	0.0601	0.093	0.0014	1493	28.37	1496.4	20.17
Z39	4183	2168	0.52	1	265513	0.253	0.0038	3.281	0.0592	0.094	0.0014	1506.5	28.62	1456.1	19.74
Z40	1516	1171	0.77	15	100315	0.265	0.0040	3.408	0.0630	0.093	0.0015	1497.1	29.67	1513	20.58
Z41	1715	837	0.49	6	115343	0.269	0.0041	3.428	0.0641	0.092	0.0015	1475.7	30.31	1536.2	20.94
Z42	2026	915	0.45	23	132630	0.262	0.0040	3.363	0.0637	0.093	0.0015	1487.6	30.65	1501.7	20.6
Z43	2622	963	0.37	14	173222	0.265	0.0041	3.393	0.0651	0.093	0.0015	1484.5	31.28	1515.8	20.84
Z44	1950	737	0.38	0	127286	0.262	0.0041	3.398	0.0665	0.094	0.0016	1508.4	31.87	1501	20.79
Z45	1756	1529	0.87	7	119578	0.275	0.0043	3.585	0.0707	0.095	0.0016	1521.8	32.08	1564.2	21.69
Z46	1759	1537	0.87	10	116323	0.266	0.0042	3.392	0.0688	0.092	0.0017	1475.9	33.6	1521.8	21.27
Z47	2753	1548	0.56	0	184668	0.270	0.0042	3.437	0.0704	0.092	0.0017	1474.4	34.06	1540.6	21.54

APPENDIX D: EQDD008A-397.3 MONAZITE ANALYSIS RESULTS TABLE

EQDD008A-397.3					Radiogenic Ratios						Age Ma					
Analysis_#	^{204}Pb	^{206}Pb	^{207}Pb	^{238}U	$^{206}Pb/^{238}U$	±	$^{207}Pb/^{235}U$	±	$^{207}Pb/^{206}Pb$	±	$^{207}Pb/^{206}Pb$	±	$^{206}Pb/^{238}U$	±	$^{207}Pb/^{235}U$	±
MZ1_1	0	31395	3029	167064	0.27971	0.00429	3.62545	0.06085	0.09407	0.00125	1509.5	24.85	1589.9	21.61	1555.1	13.36
MZ1_2	3	113054	10883	617694	0.27275	0.00411	3.52747	0.05502	0.09386	0.00108	1505.3	21.5	1554.8	20.83	1533.4	12.34
MZ2_1	0	30853	2962	167117	0.27615	0.00424	3.56401	0.0591	0.09366	0.00121	1501.2	24.14	1571.9	21.4	1541.6	13.15
MZ2_2	0	39781	3900	226337	0.26395	0.00404	3.483	0.05639	0.09576	0.00117	1543	22.76	1510	20.6	1523.4	12.77
MZ3_1	0	51290	4902	294151	0.26457	0.00407	3.40874	0.05442	0.0935	0.00109	1497.9	21.8	1513.2	20.73	1506.4	12.53
MZ3_2	9	31805	3097	183517	0.26091	0.00402	3.42254	0.05652	0.09519	0.0012	1531.9	23.58	1494.5	20.53	1509.6	12.98
MZ4_1	3	147047	14168	854269	0.25984	0.00395	3.37829	0.05277	0.09434	0.00105	1515	20.9	1489	20.24	1499.4	12.24
MZ4_2	0	29124	2820	162958	0.26819	0.00414	3.49003	0.05923	0.09444	0.00126	1516.9	25.02	1531.6	21.07	1525	13.4
MZ5_1	0	34028	3286	186380	0.27707	0.00429	3.60611	0.05935	0.09445	0.00117	1517.1	23.14	1576.6	21.64	1550.9	13.08
MZ5_2	2	31474	3048	178451	0.26613	0.00412	3.46644	0.0582	0.09452	0.00123	1518.6	24.31	1521.1	20.96	1519.6	13.23
MZ6_1	3	31725	3089	174490	0.26696	0.004	3.49568	0.05562	0.09502	0.00116	1528.6	22.88	1525.4	20.37	1526.2	12.56
MZ6_2	5	166984	15813	887484	0.27553	0.00406	3.50668	0.05249	0.09237	0.001	1474.9	20.56	1568.8	20.54	1528.7	11.83
MZ7_1	0	40761	3887	218680	0.27267	0.00408	3.50277	0.0563	0.09323	0.00117	1492.6	23.49	1554.3	20.67	1527.8	12.7
MZ7_2	29	37356	3596	207119	0.26551	0.00399	3.43808	0.05503	0.09397	0.00116	1507.6	23.08	1518	20.33	1513.1	12.59
MZ8_1	1	23107	2206	128313	0.26585	0.00404	3.41353	0.05699	0.09318	0.00124	1491.6	24.9	1519.7	20.59	1507.5	13.11
MZ8_2	1	23464	2238	129762	0.26886	0.00412	3.45819	0.05813	0.09334	0.00124	1494.8	24.89	1535	20.91	1517.7	13.24
MZ9_1	0	32349	3144	180713	0.2652	0.00403	3.47312	0.05724	0.09504	0.00122	1528.8	24.02	1516.4	20.53	1521.1	12.99
MZ9_2	14	26473	2581	144820	0.27299	0.0042	3.59331	0.06085	0.09551	0.00127	1538.3	24.89	1555.9	21.26	1548.1	13.45
MZ10_1	0	56032	5509	309352	0.2699	0.00409	3.56511	0.05726	0.09586	0.00116	1544.9	22.63	1540.3	20.78	1541.8	12.74
MZ10_2	13	148590	14456	797206	0.27849	0.00421	3.64377	0.0573	0.09494	0.00109	1527	21.57	1583.7	21.22	1559.1	12.53
MZ11_1	15	61046	5876	330259	0.27876	0.00426	3.63369	0.05771	0.09459	0.00109	1520	21.66	1585.1	21.47	1556.9	12.65
MZ11_2	20	57279	5661	321940	0.26887	0.00412	3.60617	0.05766	0.09733	0.00114	1573.6	21.69	1535	20.93	1550.9	12.71
MZ12_1	0	45502	4364	255145	0.26917	0.00413	3.50262	0.05666	0.09443	0.00113	1516.7	22.44	1536.6	20.98	1527.8	12.78
MZ12_2	0	48219	4723	266254	0.27344	0.0042	3.6399	0.0592	0.0966	0.00117	1559.5	22.52	1558.2	21.26	1558.3	12.96
MZ12_3	0	31721	3058	176013	0.27199	0.0042	3.56332	0.05955	0.09507	0.00121	1529.5	23.87	1550.9	21.29	1541.4	13.25
MZ13_1	20	41221	3992	231983	0.26867	0.00414	3.53651	0.05797	0.09552	0.00117	1538.4	22.87	1534.1	21.02	1535.4	12.97
MZ13_2	0	66519	6288	370081	0.27145	0.00416	3.49511	0.05665	0.09344	0.00112	1496.8	22.45	1548.2	21.09	1526.1	12.8

APPENDIX D: EQDD008A-397.3 MONAZITE ANALYSIS RESULTS TABLE-CONTINUED

EQDD008A-397.3					Radiogenic Ratios						Age Ma					
Analysis_#	^{204}Pb	^{206}Pb	^{207}Pb	^{238}U	$^{206}Pb/^{238}U$	±	$^{207}Pb/^{235}U$	±	$^{207}Pb/^{206}Pb$	±	$^{207}Pb/^{206}Pb$	±	$^{206}Pb/^{238}U$	±	$^{207}Pb/^{235}U$	±
MZ13_3	0	66687	6355	369093	0.2746	0.00423	3.55937	0.05771	0.09406	0.00111	1509.4	22.2	1564.1	21.39	1540.5	12.85
MZ14_1	6	95021	9104	528957	0.27903	0.00436	3.62922	0.05781	0.09439	0.00103	1515.9	20.46	1586.5	21.98	1556	12.68
MZ14_2	0	231679	21804	1290823	0.26903	0.00408	3.46144	0.05543	0.0934	0.0011	1495.9	22.08	1535.9	20.71	1518.5	12.61
MZ14_3	3	172620	16291	950597	0.27465	0.0042	3.54212	0.05702	0.09359	0.00109	1499.9	21.95	1564.4	21.23	1536.7	12.75
MZ14_4	0	141977	13653	782705	0.27486	0.00421	3.60932	0.05822	0.09529	0.00112	1533.9	21.89	1565.4	21.29	1551.6	12.83
MZ15_1	0	38206	3767	208198	0.2678	0.00399	3.59618	0.05742	0.09744	0.0012	1575.6	22.85	1529.6	20.29	1548.7	12.68
MZ15_2	0	38101	3683	212398	0.26203	0.00391	3.44855	0.05522	0.09549	0.00118	1537.8	23.05	1500.2	19.96	1515.5	12.6
MZ16_1	11	79869	7628	438522	0.26671	0.00395	3.46483	0.05377	0.09426	0.00109	1513.3	21.65	1524.1	20.13	1519.2	12.23
MZ16_2	0	51807	4997	279666	0.27137	0.00405	3.56002	0.05657	0.09518	0.00115	1531.7	22.63	1547.8	20.52	1540.7	12.6
MZ17_1	0	162430	15520	866019	0.275	0.00407	3.57186	0.05486	0.09424	0.00106	1513	21.13	1566.1	20.58	1543.3	12.18
MZ17_2	14	155427	14682	855678	0.26711	0.00397	3.42726	0.05305	0.0931	0.00106	1489.9	21.44	1526.1	20.19	1510.7	12.17
MZ17_3	0	200392	19023	1098780	0.26862	0.00399	3.45987	0.05354	0.09345	0.00106	1497.1	21.36	1533.8	20.3	1518.1	12.19
MZ18_1	0	57972	5598	301040	0.28402	0.00427	3.72062	0.05985	0.09505	0.00117	1529.1	22.95	1611.6	21.42	1575.8	12.87
MZ18_2	0	63399	6108	350381	0.2673	0.00402	3.49453	0.05642	0.09486	0.00117	1525.3	23.05	1527.1	20.45	1526	12.75
MZ19_1	16	56532	5353	308499	0.2714	0.0041	3.48393	0.05672	0.09315	0.00116	1490.9	23.44	1547.9	20.78	1523.6	12.84
MZ19_2	0	48324	4627	267972	0.26781	0.00407	3.47	0.05728	0.09402	0.0012	1508.4	23.93	1529.7	20.67	1520.4	13.01

APPENDIX E: EQDD008A-438.4 MONAZITE ANALYSIS RESULTS TABLE

EQDD008A-438.4					Radiogenic Ratios						Age Ma					
Analysis_#	^{204}Pb	^{206}Pb	^{207}Pb	^{238}U	$^{206}Pb/^{238}U$	±	$^{207}Pb/^{235}U$	±	$^{207}Pb/^{206}Pb$	±	$^{207}Pb/^{206}Pb$	±	$^{206}Pb/^{238}U$	±	$^{207}Pb/^{235}U$	±
MON1RIM_07	0	281630	26410	1571394	0.26117	0.00383	3.27887	0.04955	0.09109	0.00102	1448.4	21.19	1495.8	19.6	1476.1	11.76
MON1CORE	17	59311	5664	336600	0.25922	0.00386	3.31815	0.05204	0.09288	0.0011	1485.3	22.47	1485.9	19.78	1485.3	12.24
MZ2C_01	0	52016	5055	289605	0.25495	0.00367	3.31702	0.0507	0.09438	0.00113	1515.7	22.4	1464	18.86	1485.1	11.92
MZ2C_02	2	41989	4005	234478	0.25676	0.00373	3.27797	0.05022	0.09262	0.0011	1480	22.4	1473.2	19.14	1475.8	11.92
MZ2C_03	8	44174	4298	239842	0.26444	0.00385	3.44645	0.05311	0.09455	0.00113	1519.1	22.36	1512.5	19.63	1515.1	12.13
MZ3C_01	0	34810	3335	194278	0.25764	0.00377	3.30498	0.05165	0.09306	0.00114	1489.1	23	1477.7	19.3	1482.2	12.18
MZ3C_02	15	41675	4002	235637	0.25301	0.00367	3.25508	0.05046	0.09333	0.00113	1494.5	22.8	1454	18.9	1470.4	12.04
MZ4C_01	8	46577	4409	253306	0.2624	0.0038	3.3299	0.05171	0.09205	0.00112	1468.4	23.14	1502.1	19.41	1488.1	12.13
MZ4C_02	0	50635	4912	282646	0.25508	0.00369	3.31712	0.05167	0.09433	0.00116	1514.7	23.08	1464.6	18.95	1485.1	12.15
MZ5C_01	4	46174	4415	263921	0.26176	0.00404	3.35372	0.05903	0.09298	0.00134	1487.5	26.97	1498.9	20.62	1493.7	13.77
MZ5C_02	21	39283	3767	225314	0.24972	0.00364	3.21407	0.05101	0.09336	0.00118	1495.3	23.71	1437	18.78	1460.6	12.29
MZ6C_01	0	52392	5035	286290	0.27305	0.00415	3.5177	0.0568	0.09351	0.00115	1498.2	23.07	1556.3	21.01	1531.2	12.77
MZ6R_01	0	182328	17030	1001625	0.27177	0.0041	3.40426	0.05311	0.09092	0.00104	1444.8	21.61	1549.8	20.77	1505.4	12.25
MZ7_01	0	179507	17292	986802	0.27175	0.0041	3.51255	0.05512	0.09382	0.00108	1504.4	21.66	1549.7	20.8	1530	12.4
MZ7_02	15	40646	3882	233414	0.26031	0.00399	3.33739	0.05564	0.09306	0.00121	1489	24.41	1491.4	20.38	1489.8	13.02
MZ8_01	0	51848	4941	281722	0.27528	0.00421	3.5239	0.0582	0.09291	0.00118	1485.9	24.08	1567.5	21.26	1532.6	13.06
MZ8_02	0	50550	4891	282317	0.26799	0.0041	3.48507	0.05792	0.09439	0.00122	1515.9	24.1	1530.6	20.84	1523.8	13.11
MZ8_03	24	50145	4833	280247	0.26797	0.00411	3.47247	0.05811	0.09405	0.00122	1509.1	24.38	1530.5	20.87	1521	13.19
MZ9_01	4	164511	15969	920628	0.26778	0.00407	3.49665	0.0567	0.09477	0.00116	1523.5	22.84	1529.5	20.69	1526.5	12.8
MZ9_02	0	47966	4764	266816	0.26956	0.00414	3.60399	0.06116	0.09703	0.00129	1567.8	24.74	1538.6	21.04	1550.4	13.49
MZ10_01	0	51600	5123	283095	0.27348	0.0042	3.65643	0.06183	0.09703	0.00128	1567.8	24.52	1558.4	21.25	1561.9	13.48
MZ10_02	0	56319	5447	304407	0.27777	0.00427	3.62014	0.06156	0.09459	0.00126	1519.8	24.88	1580.1	21.53	1554	13.53
MZ10_03	0	52084	5031	285913	0.27366	0.00422	3.56367	0.06168	0.0945	0.0013	1518.2	25.64	1559.4	21.36	1541.5	13.72
MZ11_01	0	56583	5471	312645	0.27131	0.00413	3.54297	0.05675	0.09475	0.00113	1523	22.32	1547.4	20.93	1536.9	12.69
MZ11_02	0	56669	5410	318757	0.26488	0.00402	3.42622	0.05577	0.09384	0.00116	1505	23.25	1514.8	20.48	1510.4	12.79
MZ11_03	0	51807	4884	283168	0.27236	0.00413	3.47819	0.05676	0.09265	0.00116	1480.5	23.58	1552.7	20.93	1522.3	12.87
MZ12_01	0	70029	6723	383951	0.27094	0.00409	3.52505	0.05684	0.09438	0.00115	1515.7	22.89	1545.6	20.74	1532.9	12.75
MZ12_02	6	315731	29989	1690433	0.27687	0.00414	3.56501	0.05596	0.0934	0.00108	1496	21.8	1575.6	20.92	1541.8	12.45
MZ13_01	0	50585	4865	281442	0.26588	0.00402	3.4682	0.05706	0.09462	0.00121	1520.5	23.92	1519.8	20.45	1520	12.97
MZ13_02	0	52270	4956	292225	0.26451	0.00399	3.39624	0.05567	0.09313	0.00119	1490.5	23.9	1512.9	20.34	1503.5	12.86
MZ14_01	18	47271	4524	262262	0.26551	0.004	3.44885	0.05738	0.09421	0.00124	1512.4	24.58	1518	20.39	1515.6	13.1
MZ14_02	0	46667	4507	253626	0.27048	0.00407	3.54672	0.05926	0.0951	0.00126	1530.2	24.78	1543.2	20.67	1537.7	13.23
MZ15_01	0	311310	29248	1631094	0.28014	0.00417	3.5741	0.05723	0.09254	0.00114	1478.3	23.21	1592.1	20.98	1543.8	12.7
MZ15_02	0	50976	4882	283666	0.26307	0.00395	3.4204	0.05761	0.09431	0.00128	1514.3	25.36	1505.6	20.16	1509.1	13.23
MZ16_01	0	116985	10924	616303	0.28272	0.00426	3.57431	0.05593	0.09175	0.00105	1462.1	21.6	1605	21.39	1543.8	12.41

APPENDIX E: EQDD008A-438.4 MONAZITE ANALYSIS RESULTS TABLE - CONTINUED

EQDD008A-438.4					Radiogenic ratios						Age Ma					
Analysis_#	^{204}Pb	^{206}Pb	^{207}Pb	^{238}U	$^{206}Pb/^{238}U$	±	$^{207}Pb/^{235}U$	±	$^{207}Pb/^{206}Pb$	±	$^{207}Pb/^{206}Pb$	±	$^{206}Pb/^{238}U$	±	$^{207}Pb/^{235}U$	±
MZ16_02	6	130031	12586	743067	0.26136	0.00394	3.42109	0.05326	0.09499	0.00107	1527.9	21.11	1496.8	20.14	1509.3	12.23
MZ17_01	1	302488	28606	1716720	0.26317	0.00396	3.36192	0.05183	0.09271	0.00103	1481.9	20.93	1506	20.2	1495.6	12.07
MZ17_02	0	217183	21117	1257652	0.25843	0.0039	3.39941	0.05279	0.09547	0.00107	1537.3	20.87	1481.8	19.97	1504.3	12.18
MZ18_01	0	51640	5144	311460	0.24813	0.00378	3.34449	0.05389	0.09782	0.00118	1582.9	22.44	1428.8	19.5	1491.5	12.59
MZ18_02	0	53321	4992	294625	0.2709	0.00413	3.42741	0.05572	0.09182	0.00113	1463.5	23.16	1545.4	20.93	1510.7	12.78
MZ18_03	12	136625	13018	758251	0.26942	0.00408	3.47012	0.05529	0.09348	0.0011	1497.5	22.17	1537.8	20.71	1520.5	12.56
MZ19_01	8	48152	4760	276176	0.26136	0.00399	3.49083	0.05724	0.09693	0.00121	1565.9	23.22	1496.8	20.41	1525.1	12.94
MZ19_02	28	97574	9347	550045	0.26632	0.00405	3.44773	0.05532	0.09395	0.00112	1507.1	22.32	1522.1	20.62	1515.4	12.63
MZ20_01	16	293659	27860	1666014	0.26453	0.00401	3.39247	0.05363	0.09307	0.00107	1489.4	21.69	1513	20.43	1502.7	12.4
MZ20_02	11	262966	25176	1510546	0.26068	0.00395	3.37763	0.05406	0.09404	0.00112	1508.9	22.24	1493.3	20.19	1499.2	12.54
MZ21_01D	16	85090	8027	455652	0.28087	0.00427	3.53522	0.0551	0.09133	0.00104	1453.3	21.44	1595.8	21.5	1535.1	12.34
MZ21_02D	0	86649	8187	483182	0.26962	0.0041	3.40005	0.05307	0.0915	0.00104	1456.9	21.5	1538.9	20.82	1504.4	12.25
MZ22_01D	0	237574	22376	1339334	0.26576	0.00401	3.34083	0.05131	0.09121	0.00101	1450.9	20.9	1519.2	20.44	1490.6	12
MZ22_02D	10	95578	9162	530263	0.26994	0.0041	3.45674	0.05432	0.09291	0.00108	1486	21.98	1540.5	20.79	1517.4	12.38
MZ22_03D	0	102718	9930	558001	0.27579	0.00419	3.55809	0.05622	0.09361	0.0011	1500.3	22.05	1570.1	21.17	1540.2	12.52
MZ23_01D	0	79652	7673	435418	0.27493	0.00419	3.53715	0.05641	0.09335	0.00111	1495.1	22.35	1565.8	21.21	1535.6	12.62
MZ23_02D	11	40754	3871	232811	0.26431	0.00407	3.36164	0.05475	0.09228	0.00113	1473.1	23.27	1511.9	20.73	1495.5	12.75
MZ24_01D	19	40705	3918	224953	0.27256	0.00419	3.51055	0.05742	0.09346	0.00116	1497.2	23.38	1553.8	21.21	1529.6	12.93
MZ24_02D	0	52023	4892	293388	0.26689	0.00409	3.36213	0.0549	0.09141	0.00113	1455	23.42	1525	20.82	1495.6	12.78
MZ25_01D	0	193211	18657	1101075	0.26267	0.00398	3.39634	0.05391	0.09382	0.00111	1504.5	22.17	1503.5	20.32	1503.6	12.45
MZ25_02D	13	160579	15516	901998	0.26673	0.00406	3.44607	0.0559	0.09375	0.00116	1503	23.14	1524.2	20.66	1515	12.77
MZ26_01	0	261256	24861	1441008	0.26959	0.00404	3.4475	0.05321	0.0928	0.00104	1483.6	21.26	1538.7	20.53	1515.3	12.15
MZ27_01	0	35090	3390	200192	0.26187	0.004	3.39973	0.05582	0.09421	0.00119	1512.3	23.71	1499.4	20.44	1504.3	12.88
MZ27_02	4	44159	4266	252298	0.26141	0.00399	3.39536	0.05539	0.09425	0.00118	1513.2	23.39	1497	20.37	1503.3	12.8
MZ28_01	31	35883	3459	201310	0.26633	0.00409	3.44962	0.05778	0.09399	0.00123	1507.9	24.58	1522.1	20.8	1515.8	13.18
MZ28_02	0	261567	25349	1482434	0.26421	0.00399	3.43747	0.05369	0.09441	0.00107	1516.3	21.3	1511.4	20.36	1513	12.29
MZ29_01	0	51953	5073	303429	0.25673	0.00393	3.36427	0.0553	0.09509	0.0012	1529.8	23.54	1473.1	20.16	1496.1	12.87
MZ29_02	0	240556	22925	1385594	0.26094	0.00396	3.34111	0.05254	0.09292	0.00106	1486	21.66	1494.6	20.24	1490.7	12.29
MZ29_03	0	40359	3862	234995	0.25842	0.00398	3.32191	0.05545	0.09328	0.0012	1493.6	24.2	1481.8	20.38	1486.2	13.03
MZ30_01	0	212269	19760	1202351	0.26574	0.00405	3.31366	0.05343	0.09049	0.00109	1435.8	22.77	1519.1	20.65	1484.3	12.58
MZ30_02	2	60669	5795	345805	0.26428	0.00408	3.37691	0.05703	0.09272	0.00122	1482.1	24.88	1511.7	20.8	1499.1	13.23

APPENDIX F: EQDD008A-459.8 MONAZITE ANALYSIS RESULTS TABLE

EQDD008A-459.8					Radiogenic Ratios						Age Ma					
Analysis_#	^{204}Pb	^{206}Pb	^{207}Pb	^{238}U	^{206}Pb/^{238}U	±	^{207}Pb/^{235}U	±	^{207}Pb/^{206}Pb	±	^{207}Pb/^{206}Pb	±	^{206}Pb/^{238}U	±	^{207}Pb/^{235}U	±
MZ1_1	0	72523	6999	394799	0.283	0.0044	3.674	0.0601	0.0942	0.0011	1511.7	22.34	1606.9	22.22	1565.7	13.05
MZ1_2	12	46393	4432	265906	0.269	0.0042	3.463	0.0579	0.0933	0.0012	1493.8	23.43	1537.7	21.5	1518.9	13.18
MZ2_1	0	44029	4252	246954	0.275	0.0043	3.585	0.0603	0.0945	0.0012	1518.2	23.55	1567.5	21.89	1546.2	13.35
MZ2_2	0	75197	7235	414452	0.280	0.0044	3.630	0.0597	0.0940	0.0011	1508.2	22.53	1592.6	22.09	1556.2	13.1
MZ3_1	0	39794	3859	221218	0.278	0.0044	3.630	0.0617	0.0948	0.0012	1524.1	24.08	1580.5	22.11	1556.1	13.54
MZ3_2	0	191533	18071	1063885	0.278	0.0043	3.539	0.0575	0.0923	0.0011	1473.4	22.06	1582.4	21.9	1536	12.87
MZ4_1	18	44945	4291	249984	0.277	0.0044	3.577	0.0609	0.0936	0.0012	1499.1	24.2	1578.4	22.04	1544.3	13.52
MZ4_2	0	45301	4388	258541	0.271	0.0043	3.541	0.0605	0.0949	0.0012	1526.9	24.17	1544	21.64	1536.4	13.52
MZ4_3	11	49489	4627	268639	0.285	0.0045	3.592	0.0615	0.0916	0.0012	1459.5	24.46	1614	22.49	1547.8	13.59
MZ5_1	21	134364	12725	770789	0.269	0.0042	3.445	0.0573	0.0929	0.0011	1486.2	23.12	1535.9	21.37	1514.7	13.09
MZ5_2	10	49662	4771	284276	0.270	0.0043	3.508	0.0606	0.0943	0.0012	1513.9	24.64	1540.8	21.63	1529.1	13.64
MZ6_1	20	53461	5208	303622	0.270	0.0042	3.512	0.0570	0.0944	0.0011	1516.7	22.41	1540.4	21.33	1530	12.83
MZ6_2	0	29259	2825	167774	0.267	0.0042	3.452	0.0585	0.0937	0.0012	1502.3	24.46	1527.3	21.36	1516.4	13.34
MZ6_3	0	43990	4265	250412	0.269	0.0042	3.496	0.0577	0.0942	0.0012	1511.4	23.16	1538	21.37	1526.4	13.04
MZ7_1	0	43759	4216	250790	0.268	0.0042	3.450	0.0571	0.0936	0.0012	1499.5	23.34	1528.3	21.25	1515.8	13.04
MZ7_2	3	106414	10095	602038	0.271	0.0042	3.449	0.0555	0.0923	0.0011	1473.7	22.08	1546.7	21.33	1515.7	12.67
MZ8_1	4	50169	4824	290630	0.265	0.0041	3.418	0.0568	0.0937	0.0012	1501.4	23.39	1514.5	21.08	1508.6	13.06
MZ8_2	0	55985	5258	316799	0.271	0.0042	3.425	0.0572	0.0916	0.0012	1459.4	23.67	1547.2	21.49	1510.1	13.13
MZ9_1	20	47582	4542	268072	0.272	0.0043	3.498	0.0588	0.0932	0.0012	1492.1	23.92	1552.5	21.58	1526.7	13.28
MZ9_2	12	53402	5065	304078	0.270	0.0042	3.443	0.0579	0.0927	0.0012	1481.1	24.02	1538.8	21.41	1514.3	13.24
MZ10_1	0	36993	3495	209744	0.271	0.0043	3.453	0.0596	0.0925	0.0012	1476.8	25.2	1545.6	21.62	1516.4	13.59
MZ10_2	0	92812	8540	559324	0.254	0.0040	3.163	0.0529	0.0902	0.0011	1429.4	23.7	1461.6	20.37	1448.1	12.91
MZ11_1	0	33923	3253	190886	0.274	0.0043	3.524	0.0598	0.0933	0.0012	1494.7	24.23	1561.1	21.86	1532.7	13.41
MZ11_2	0	32599	3100	183808	0.274	0.0043	3.495	0.0595	0.0926	0.0012	1480.3	24.51	1559.9	21.88	1526	13.44
MZ11_3	8	42608	4036	236286	0.278	0.0044	3.541	0.0592	0.0923	0.0012	1473.6	23.62	1583.3	22.07	1536.5	13.23
MZ12_1	0	32385	3136	184152	0.271	0.0043	3.532	0.0603	0.0945	0.0012	1517.8	24.39	1547.2	21.71	1534.4	13.51
MZ13_1	0	44470	4125	254266	0.270	0.0042	3.370	0.0566	0.0906	0.0011	1437.6	23.79	1540.7	21.55	1497.4	13.15
MZ13_2	20	35153	3455	206868	0.262	0.0041	3.466	0.0593	0.0960	0.0013	1548.3	24.35	1499.9	21.11	1519.6	13.47
MZ14_1	0	42736	4066	250992	0.263	0.0041	3.373	0.0573	0.0932	0.0012	1492.6	24.15	1502.8	21.09	1498.2	13.31
MZ15_1	14	43632	4211	249353	0.270	0.0043	3.519	0.0598	0.0946	0.0012	1520.8	24.02	1540.1	21.55	1531.6	13.44
MZ15_2	15	106725	10167	603413	0.273	0.0043	3.513	0.0580	0.0934	0.0011	1496.9	22.63	1554.9	21.58	1530.1	13.04
MZ16_1	8	57250	5455	325500	0.271	0.0043	3.501	0.0593	0.0936	0.0012	1500.9	23.8	1547.5	21.6	1527.5	13.37
MZ16_2	0	22178	2113	125825	0.272	0.0043	3.514	0.0638	0.0938	0.0014	1503.8	27.2	1550.3	21.99	1530.3	14.35
MZ17_1	16	48612	4627	280198	0.267	0.0042	3.449	0.0593	0.0936	0.0012	1500.3	24.59	1527.3	21.39	1515.6	13.54
MZ17_2	9	45687	4342	264590	0.266	0.0042	3.429	0.0592	0.0935	0.00124	1497	24.8	1521.8	21.35	1511	13.58

APPENDIX G: RDD003-262 MONAZITE ANALYSIS RESULTS TABLE

RDD003-262					Radiogenic Ratios						Age Ma					
Analysis_#	^{204}Pb	^{206}Pb	^{207}Pb	^{238}U	$^{206}Pb/^{238}U$	±	$^{207}Pb/^{235}U$	±	$^{207}Pb/^{206}Pb$	±	$^{207}Pb/^{206}Pb$	±	$^{206}Pb/^{238}U$	±	$^{207}Pb/^{235}U$	±
1	27	299923	29280	1699702	0.284	0.0046	3.708	0.0589	0.095	0.00096	1520.2	19.03	1613.5	23.07	1573.1	12.69
2	0	318428	31376	1875889	0.274	0.0044	3.606	0.0573	0.095	0.00097	1536.9	18.98	1561.9	22.46	1550.9	12.64
3	14	232779	22677	1371871	0.275	0.0045	3.574	0.0572	0.094	0.00097	1516.6	19.24	1564.5	22.56	1543.8	12.7
4	18	274954	27796	1624069	0.275	0.0045	3.711	0.0595	0.098	0.001	1585.2	18.97	1565.9	22.65	1573.7	12.81
5	29	273742	26668	1626581	0.274	0.0045	3.565	0.0573	0.094	0.00097	1515.8	19.2	1561.5	22.65	1541.8	12.75
6	19	312180	30434	1859590	0.274	0.0045	3.569	0.0575	0.094	0.00097	1517.2	19.17	1561.9	22.72	1542.6	12.78
7	3	283526	27249	1730250	0.268	0.0044	3.444	0.0558	0.093	0.00096	1490.4	19.33	1532.4	22.41	1514.5	12.74
8	34	241149	23668	1400304	0.283	0.0047	3.707	0.0603	0.095	0.00098	1530.1	19.34	1605.5	23.42	1572.8	13.01
9	17	227328	22609	1323667	0.283	0.0047	3.756	0.0614	0.096	0.001	1555.1	19.35	1605.6	23.49	1583.5	13.1
10	39	321586	31306	1970120	0.270	0.0045	3.505	0.0573	0.094	0.00097	1515	19.34	1538.6	22.68	1528.3	12.92
11	9	251103	24849	1529226	0.272	0.0045	3.594	0.0591	0.096	0.001	1545.9	19.42	1550.6	22.91	1548.2	13.06
12	5	278137	27996	1685417	0.274	0.0046	3.685	0.0608	0.098	0.00101	1577.9	19.34	1561.4	23.12	1568.1	13.17
13	0	397278	38683	2402378	0.275	0.0046	3.582	0.0592	0.094	0.00098	1515.6	19.43	1568.3	23.26	1545.6	13.11
14	34	406684	40273	2368023	0.281	0.0046	3.740	0.0607	0.096	0.00099	1556.6	19.1	1598.6	23.26	1580	13
15	12	504816	50213	2990266	0.277	0.0046	3.695	0.0599	0.097	0.00099	1562.8	19.01	1576.7	23.01	1570.2	12.96
16	42	542012	52162	3347315	0.266	0.0044	3.430	0.0557	0.094	0.00095	1498.4	19.17	1521.5	22.33	1511.3	12.76
17	8	414465	41212	2429185	0.281	0.0046	3.736	0.0608	0.097	0.00099	1557.8	19.1	1596.1	23.35	1579.2	13.03
18	24	390733	38344	2357961	0.273	0.0045	3.583	0.0584	0.095	0.00098	1530.9	19.21	1557.5	22.89	1545.8	12.94
19	28	496419	48618	2882103	0.285	0.0047	3.719	0.0606	0.095	0.00097	1525	19.17	1614.2	23.65	1575.4	13.04
20	25	428747	41652	2697608	0.263	0.0044	3.405	0.0556	0.094	0.00097	1507.6	19.29	1505.1	22.28	1505.6	12.82
21	9	401236	40246	2426190	0.274	0.0046	3.669	0.0601	0.097	0.001	1570.2	19.21	1561.1	23.05	1564.5	13.08
22	22	443405	42854	2736829	0.269	0.0045	3.463	0.0568	0.093	0.00096	1494.5	19.38	1537.1	22.8	1518.8	12.92
23	24	416388	40963	2642738	0.262	0.0044	3.421	0.0561	0.095	0.00098	1523.9	19.36	1499.6	22.32	1509.2	12.88
24	11	423939	41649	2513974	0.281	0.0047	3.656	0.0600	0.095	0.00098	1519.1	19.36	1594.4	23.59	1561.9	13.08
25	17	378088	36692	2216951	0.284	0.0048	3.658	0.0603	0.093	0.00097	1494.8	19.56	1613.5	23.9	1562.2	13.13
26	26	375772	36718	2288475	0.280	0.0048	3.650	0.0612	0.095	0.00096	1520.5	19.05	1591	24.1	1560.5	13.35
27	33	394882	37827	2499939	0.269	0.0046	3.445	0.0577	0.093	0.00094	1483.3	19.23	1537.9	23.39	1514.6	13.19
28	22	336040	32902	2071316	0.278	0.0048	3.637	0.0614	0.095	0.00097	1526.2	19.12	1582	24.11	1557.6	13.44
29	21	451460	43292	2855511	0.270	0.0046	3.453	0.0579	0.093	0.00094	1483.7	19.23	1541	23.46	1516.6	13.2
30	23	290917	29424	1765822	0.282	0.0048	3.797	0.0639	0.098	0.001	1583.5	19.04	1599.4	24.28	1592	13.52
31	3	303212	30325	1838312	0.282	0.0048	3.757	0.0632	0.097	0.00099	1561.7	19.13	1600.9	24.3	1583.6	13.5
32	24	328871	31920	2052485	0.274	0.0047	3.546	0.0597	0.094	0.00096	1504.5	19.26	1562.3	23.81	1537.4	13.34
33	39	261497	25843	1621439	0.276	0.0048	3.635	0.0614	0.095	0.00099	1537.8	19.31	1572.3	23.98	1557.2	13.45
34	10	268301	26959	1652913	0.278	0.0048	3.720	0.0629	0.097	0.001	1568.2	19.25	1582.3	24.13	1575.8	13.53
35	36	284448	28063	1730823	0.282	0.0049	3.700	0.0626	0.095	0.00099	1533.1	19.36	1600.7	24.39	1571.3	13.52
36	7	330386	33122	2060708	0.275	0.0047	3.669	0.0621	0.097	0.001	1562.5	19.25	1566.9	23.95	1564.6	13.5
37	19	276506	27575	1723120	0.276	0.0048	3.654	0.0620	0.09621	0.001	1551.9	19.4	1569.1	24.01	1561.3	13.52

APPENDIX H: RDD003-267.3 MONAZITE ANALYSIS RESULTS TABLE

RDD003-267.3					Radiogenic Ratios						Age Ma					
Analysis_ #	^{204}Pb	^{206}Pb	^{207}Pb	^{238}U	$^{206}Pb/^{238}U$	±	$^{207}Pb/^{235}U$	±	$^{207}Pb/^{206}Pb$	±	$^{207}Pb/^{206}Pb$	±	$^{206}Pb/^{238}U$	±	$^{207}Pb/^{235}U$	±
1	6	441487	43162	2456667	0.287	0.0046	3.740	0.058	0.095	0.00095	1519.3	18.74	1626.4	23	1580	12.52
2	7	308885	31010	1791672	0.275	0.0044	3.685	0.058	0.097	0.00098	1569.6	18.75	1567.6	22.27	1568.1	12.51
3	18	379847	37035	2131742	0.285	0.0046	3.700	0.058	0.094	0.00095	1515	18.85	1614.1	22.85	1571.3	12.51
4	7	369524	35393	2192514	0.269	0.0043	3.438	0.054	0.093	0.00093	1481.6	19.09	1536.3	21.88	1513.2	12.33
5	17	323900	31092	1921979	0.269	0.0043	3.446	0.054	0.093	0.00094	1486.2	19.18	1536.2	21.88	1515	12.35
6	3	366972	36372	2129783	0.275	0.0044	3.639	0.057	0.096	0.00097	1547.1	18.87	1566.7	22.26	1558	12.5
7	25	322794	31435	1847974	0.279	0.0045	3.625	0.057	0.094	0.00096	1514.4	19.04	1585.8	22.5	1555	12.51
8	16	329405	32400	1856009	0.283	0.0045	3.721	0.059	0.095	0.00097	1533.6	19.02	1608.3	22.79	1575.9	12.59
9	21	519084	49802	3037279	0.273	0.0044	3.496	0.055	0.093	0.00094	1486.9	19.2	1555.3	22.11	1526.2	12.4
10	0	416090	39836	2457456	0.270	0.0043	3.456	0.054	0.093	0.00094	1483.3	19.29	1542.4	21.96	1517.3	12.4
11	8	435571	43181	2446996	0.284	0.0046	3.763	0.059	0.096	0.00098	1549.6	19.03	1612.3	22.83	1585	12.64
12	25	358223	35677	2079502	0.275	0.0044	3.660	0.058	0.097	0.00099	1558.7	19.12	1566.2	22.26	1562.6	12.59
13	12	349871	34674	1973867	0.278	0.0044	3.671	0.056	0.096	0.00096	1540.6	18.8	1583.8	22.12	1565	12.28
14	0	374428	37332	2155277	0.273	0.0043	3.615	0.056	0.096	0.00097	1552.1	18.78	1554.1	21.72	1552.9	12.23
15	22	374965	37253	2189682	0.268	0.0042	3.547	0.055	0.096	0.00097	1545.6	18.83	1532.6	21.43	1537.7	12.17
16	14	335317	33205	1953477	0.269	0.0042	3.540	0.054	0.096	0.00097	1539.7	18.93	1534.2	21.43	1536.2	12.17
17	0	268684	26469	1444988	0.291	0.0046	3.810	0.059	0.095	0.00097	1530.1	19.1	1645.1	22.78	1594.9	12.39
18	4	359260	36305	2093634	0.268	0.0042	3.603	0.055	0.098	0.00099	1578.1	18.9	1530.4	21.34	1550.2	12.21
19	8	345361	34904	2048852	0.263	0.0041	3.536	0.054	0.098	0.00100	1578.6	18.96	1504.7	21	1535.2	12.16
20	5	251204	24864	1446152	0.271	0.0042	3.564	0.055	0.096	0.00099	1539.7	19.26	1543.8	21.47	1541.6	12.22
21	0	393051	39054	2236030	0.273	0.0043	3.617	0.056	0.096	0.00098	1547	19.12	1558.5	21.61	1553.2	12.21
22	9	368832	37417	2117693	0.271	0.0042	3.655	0.056	0.098	0.00101	1586.2	19.1	1544.1	21.41	1561.5	12.25
23	16	351520	34138	2009835	0.271	0.0042	3.509	0.054	0.094	0.00097	1504.4	19.41	1548.2	21.44	1529.3	12.15
24	21	325968	32885	1871403	0.282	0.0046	3.781	0.060	0.098	0.00098	1577	18.77	1599	22.94	1588.8	12.72
25	6	310865	31397	1784168	0.282	0.0046	3.786	0.060	0.098	0.00099	1579.1	18.8	1599	22.94	1589.7	12.73
26	3	263960	25717	1592602	0.268	0.0043	3.473	0.055	0.094	0.00096	1511.5	19.06	1529.2	22.05	1521.1	12.51
27	15	355229	35629	2101348	0.273	0.0044	3.646	0.058	0.097	0.00098	1566.1	18.82	1555.9	22.38	1559.5	12.62
28	2	330419	33964	1952850	0.273	0.0044	3.739	0.059	0.099	0.00101	1611.2	18.77	1557.5	22.41	1579.8	12.7
29	14	256119	25386	1447165	0.286	0.0046	3.770	0.060	0.096	0.00098	1543.9	19.05	1619.7	23.19	1586.3	12.75
30	17	769785	72811	4611861	0.269	0.0044	3.392	0.054	0.091	0.00092	1455.2	19.02	1537.3	22.11	1502.5	12.39
31	4	252707	24678	1449239	0.281	0.0046	3.658	0.058	0.094	0.00097	1515.8	19.19	1597.8	22.9	1562.2	12.68
32	29	330513	31614	1966126	0.271	0.0044	3.453	0.055	0.092	0.00094	1476.5	19.33	1546.3	22.23	1516.5	12.5
33	11	266104	25435	1596708	0.269	0.0044	3.420	0.054	0.092	0.00095	1475.2	19.45	1534.1	22.08	1509	12.49
34	2	305398	29199	1841132	0.267	0.0043	3.404	0.054	0.092	0.00095	1475.7	19.43	1527.3	21.98	1505.3	12.47
35	7	218766	21474	1271501	0.277	0.0045	3.624	0.058	0.095	0.00098	1525.6	19.36	1577.4	22.63	1554.8	12.69
36	0	270008	25469	1596889	0.273	0.0044	3.420	0.055	0.091	0.00094	1446.5	19.55	1554.6	22.36	1508.9	12.52
37	7	268762	26638	1646190	0.263	0.0043	3.472	0.055	0.096	0.00099	1542	19.33	1506.5	21.74	1520.8	12.57

APPENDIX I: RDD003-292.2 MONAZITE ANALYSIS RESULTS TABLE

RDD003-292.2					Radiogenic Ratios						Age Ma					
Analysis_#	^{204}Pb	^{206}Pb	^{207}Pb	^{238}U	$^{206}Pb/^{238}U$	±	$^{207}Pb/^{235}U$	±	$^{207}Pb/^{206}Pb$	±	$^{207}Pb/^{206}Pb$	±	$^{206}Pb/^{238}U$	±	$^{207}Pb/^{235}U$	±
1	16	610307	59088	3954185	0.257	0.0043	3.342	0.055	0.094	0.00096	1515.2	19.16	1475	22.01	1491	12.88
2	8	738329	71851	4676464	0.264	0.0044	3.448	0.057	0.095	0.00097	1525.1	19.15	1509.4	22.54	1515.4	13.02
3	18	273208	29251	1579941	0.291	0.0049	4.175	0.070	0.104	0.00108	1700.8	18.93	1645	24.49	1669.2	13.67
4	17	353674	36132	2042669	0.296	0.0051	4.058	0.069	0.099	0.00103	1612.2	19.27	1673.3	25.31	1646	13.86
5	19	771293	75216	4783822	0.269	0.0045	3.516	0.059	0.095	0.00102	1524.1	20.07	1536.8	22.94	1530.8	13.27
6	12	571468	56081	3621352	0.268	0.0046	3.527	0.059	0.096	0.00099	1539.6	19.32	1529.4	23.16	1533.2	13.33
7	16	206822	20217	1267026	0.278	0.0048	3.647	0.062	0.095	0.00101	1532	19.79	1581.2	23.98	1559.8	13.58
8	6	234344	22962	1480807	0.270	0.0046	3.555	0.061	0.095	0.00101	1536.9	19.79	1542.4	23.53	1539.6	13.55
9	9	518460	50355	3202489	0.277	0.0048	3.613	0.062	0.095	0.00100	1522	19.7	1575.7	23.99	1552.5	13.59
10	30	340677	33618	2018988	0.290	0.0050	3.842	0.066	0.096	0.00102	1551.3	19.79	1640.9	24.98	1601.6	13.87
11	9	437138	44311	2675325	0.282	0.0049	3.843	0.066	0.099	0.00105	1601.6	19.6	1602.7	24.6	1601.9	13.93
12	29	877561	85090	5717719	0.265	0.0046	3.456	0.060	0.095	0.00100	1519.7	19.89	1516.2	23.42	1517.2	13.65
13	33	850855	82651	5449676	0.272	0.0048	3.552	0.062	0.095	0.00101	1522.9	19.93	1551.1	24.11	1538.9	13.85
14	19	510604	49193	3165086	0.281	0.0049	3.603	0.061	0.093	0.00094	1488.4	18.99	1596.3	24.68	1550.2	13.54
15	14	412275	39572	2570713	0.279	0.0049	3.569	0.061	0.093	0.00094	1481.7	19.23	1588	24.57	1542.7	13.54
16	29	792937	75717	5185150	0.266	0.0047	3.388	0.058	0.092	0.00093	1472	19.13	1522.9	23.68	1501.6	13.37
17	23	616132	60466	4049673	0.265	0.0046	3.466	0.059	0.095	0.00096	1524.1	18.98	1516.6	23.61	1519.5	13.46
18	14	403962	39384	2527654	0.279	0.0049	3.619	0.062	0.094	0.00096	1511.8	19.19	1585.1	24.57	1553.6	13.64
19	12	594088	56681	3894013	0.266	0.0046	3.380	0.058	0.092	0.00094	1472.2	19.38	1519.7	23.65	1499.7	13.42
20	21	521026	50465	3432466	0.264	0.0046	3.411	0.059	0.094	0.00097	1502	19.36	1511	23.5	1506.9	13.47
21	17	421649	40010	2739546	0.268	0.0047	3.395	0.058	0.092	0.00095	1462.7	19.46	1532.8	23.86	1503.3	13.49
22	21	417313	42075	2487283	0.292	0.0051	3.932	0.068	0.098	0.00101	1579.1	19.16	1652.7	25.46	1620.3	13.91
23	3	590772	57057	3833942	0.269	0.0047	3.465	0.060	0.093	0.00097	1494.7	19.45	1537.7	23.98	1519.4	13.59
24	9	567893	54796	3698098	0.269	0.0047	3.452	0.060	0.093	0.00097	1493.1	19.54	1533.7	23.94	1516.4	13.61
25	13	478353	46834	2990672	0.279	0.0049	3.651	0.063	0.095	0.00096	1526.5	18.92	1586.9	24.59	1560.7	13.64
26	2	354233	34232	2230469	0.277	0.0049	3.585	0.062	0.094	0.00096	1503.2	19.17	1578.7	24.52	1546.3	13.66
27	29	451838	43191	2887990	0.273	0.0048	3.486	0.060	0.093	0.00094	1483.1	19.29	1554.3	24.12	1524.1	13.53
28	27	430567	41880	2776791	0.270	0.0047	3.513	0.060	0.094	0.00096	1516.5	19.16	1540.8	23.92	1530.2	13.56
29	19	490797	47245	3130052	0.272	0.0048	3.510	0.060	0.093	0.00096	1497.8	19.24	1553.4	24.04	1529.6	13.55
30	12	320048	30955	2088401	0.266	0.0046	3.443	0.059	0.094	0.00097	1507.4	19.42	1519.9	23.56	1514.3	13.51
31	12	537300	51872	3500085	0.266	0.0046	3.439	0.059	0.094	0.00097	1505.5	19.36	1519.6	23.5	1513.3	13.48
32	18	268583	26417	1707176	0.272	0.0047	3.585	0.062	0.096	0.00100	1541.1	19.57	1550.6	23.9	1546.1	13.65
33	19	261354	25499	1595779	0.283	0.0049	3.694	0.063	0.095	0.00099	1525	19.63	1604.4	24.59	1570	13.71
34	14	226543	22256	1281456	0.304	0.0053	4.011	0.069	0.096	0.00101	1539.9	19.79	1713.5	26.02	1636.5	13.98
35	28	380390	36487	2349172	0.277	0.0048	3.564	0.061	0.093	0.00098	1492.6	19.7	1578.2	24.06	1541.5	13.51
36	14	445708	42842	2772287	0.276	0.0048	3.557	0.061	0.094	0.00099	1499.7	19.8	1570.3	23.99	1540	13.57

APPENDIX J: RDD003-309.2 MONAZITE ANALYSIS RESULTS TABLE

RDD003-309.2					Radiogenic Ratios						Age Ma					
Analysis_#	^{204}Pb	^{206}Pb	^{207}Pb	^{238}U	^{206}Pb/^{238}U	±	^{207}Pb/^{235}U	±	^{207}Pb/^{206}Pb	±	^{207}Pb/^{206}Pb	±	^{206}Pb/^{238}U	±	^{207}Pb/^{235}U	±
1	5	659397	63596	4243162	0.271	0.0047	3.473	0.0590	0.0931	0.00093	1490.6	18.88	1544	23.95	1521	13.4
2	19	538502	51776	3555414	0.264	0.0046	3.372	0.0574	0.0929	0.00094	1485.2	19.12	1507.8	23.44	1497.8	13.32
3	704	564386	65709	3555269	0.276	0.0048	4.276	0.0727	0.1125	0.00113	1840	18.12	1570.8	24.28	1688.8	13.98
4	33	447274	43960	2808144	0.277	0.0048	3.619	0.0616	0.0950	0.00096	1527.8	19	1574.2	24.31	1553.8	13.54
5	15	611733	59702	4015155	0.264	0.0046	3.435	0.0584	0.0944	0.00095	1515.1	18.97	1511.9	23.43	1512.6	13.36
6	20	585238	56096	3802730	0.267	0.0046	3.406	0.0579	0.0927	0.00094	1481.4	19.22	1524.3	23.58	1505.8	13.34
7	18	485516	46255	3062108	0.275	0.0048	3.485	0.0593	0.0922	0.00094	1470.4	19.35	1563.9	24.1	1523.9	13.42
8	14	547005	52880	3553416	0.266	0.0046	3.431	0.0583	0.0935	0.00095	1498.7	19.17	1522	23.51	1511.6	13.36
9	9	630678	59768	3939814	0.276	0.0048	3.492	0.0593	0.0917	0.00094	1461.4	19.34	1573.4	24.17	1525.4	13.41
10	16	613827	59395	3899169	0.271	0.0047	3.503	0.0595	0.0937	0.00096	1502.2	19.28	1548	23.79	1527.9	13.41
11	13	435024	41354	2732967	0.274	0.0047	3.477	0.0592	0.0921	0.00095	1469.1	19.64	1561.8	23.96	1522	13.42
12	32	461159	44411	2911843	0.273	0.0047	3.503	0.0596	0.0933	0.00097	1494.4	19.52	1553.7	23.83	1527.8	13.44
13	26	584503	56407	3632889	0.287	0.0052	3.652	0.0635	0.0922	0.00094	1472	19.32	1628.6	25.77	1561	13.85
14	2	550915	53346	3528234	0.279	0.0050	3.554	0.0618	0.0926	0.00094	1479	19.34	1584.7	25.14	1539.4	13.77
15	0	505887	49550	3220814	0.280	0.0050	3.614	0.0628	0.0936	0.00096	1500.9	19.25	1591.9	25.22	1552.6	13.83
16	17	658937	63518	4193726	0.280	0.0050	3.553	0.0617	0.0921	0.00095	1470.1	19.48	1590.8	25.18	1539.1	13.77
17	14	595669	56835	3892374	0.272	0.0049	3.424	0.0595	0.0912	0.00094	1451.1	19.47	1553	24.64	1509.8	13.66
18	11	384053	36771	2498704	0.273	0.0049	3.447	0.0601	0.0915	0.00095	1457.7	19.68	1557.5	24.69	1515.2	13.71
19	0	427529	40932	2767018	0.275	0.0049	3.465	0.0604	0.0916	0.00095	1458.6	19.7	1564.1	24.77	1519.3	13.73
20	24	604169	58436	3917424	0.274	0.0049	3.491	0.0608	0.0925	0.00096	1477.6	19.74	1560.7	24.7	1525.3	13.75
21	5	559637	53744	3678637	0.270	0.0048	3.413	0.0595	0.0918	0.00096	1463.8	19.79	1539.4	24.37	1507.4	13.68
22	28	507317	49810	3340214	0.269	0.0048	3.484	0.0607	0.0940	0.00099	1509	19.76	1534.9	24.27	1523.5	13.76
23	0	467190	44867	3054626	0.271	0.0048	3.430	0.0599	0.0920	0.00098	1466.5	19.99	1544.3	24.4	1511.4	13.73
24	14	530044	51001	3439226	0.272	0.0048	3.456	0.0604	0.0921	0.00098	1469.5	20.28	1552.2	24.47	1517.2	13.77
25	22	429891	41640	2644525	0.284	0.0050	3.683	0.0637	0.0943	0.00098	1513	19.41	1609.8	24.93	1567.7	13.8
26	0	459397	44876	2851496	0.285	0.0051	3.727	0.0651	0.0949	0.00098	1525.6	19.27	1616.8	25.37	1577.2	13.99
27	18	649890	62244	4231070	0.271	0.0048	3.479	0.0603	0.0932	0.00094	1492	18.94	1545.2	24.26	1522.4	13.66
28	14	523141	49259	3329497	0.277	0.0049	3.500	0.0607	0.0917	0.00093	1460.3	19.11	1576.6	24.7	1527.1	13.7
29	24	203559	20628	1163766	0.308	0.0055	4.194	0.0732	0.0987	0.00102	1599.5	19.11	1732.9	26.87	1672.9	14.31
30	7	507884	49254	3364640	0.266	0.0047	3.465	0.0602	0.0945	0.00096	1517.6	19.04	1521.2	23.93	1519.2	13.69
31	19	506375	48948	3327507	0.268	0.0047	3.483	0.0606	0.0942	0.00096	1512.1	19.1	1532.2	24.09	1523.3	13.72
32	26	509614	48246	3305918	0.272	0.0048	3.456	0.0602	0.0923	0.00094	1473.2	19.37	1549.7	24.33	1517.3	13.71
33	17	468920	45269	2968373	0.278	0.0049	3.613	0.0630	0.0941	0.00096	1511	19.23	1583.7	24.8	1552.3	13.87
34	12	403551	38429	2596105	0.274	0.0048	3.508	0.0613	0.0929	0.00096	1485.6	19.52	1561.1	24.5	1528.9	13.8
35	1	354685	34405	2286024	0.273	0.0048	3.554	0.0623	0.0946	0.001	1520.6	19.7	1553.8	24.34	1539.4	13.89
36	11	569541	54575	3763306	0.267	0.0047	3.438	0.0601	0.0935	0.00097	1498.9	19.39	1524.3	23.98	1513.2	13.75
37	13	550855	53691	3685848	0.263	0.0047	3.455	0.0605	0.0952	0.00099	1531.7	19.37	1507.2	23.74	1517	13.79